

Kondo-Majorana coupling in Double Quantum Dots.

by

Jesús David Cifuentes Pardo

Advisor: Luis Gregorio Dias da Silva

MASTER OF SCIENCE

in

Instituto de Física

(Condensed Matter Physics)

UNIVERSIDADE DE SÃO PAULO

(R. do Matão, 1371 - Butantã, São Paulo)

January 2, 2019

© Jesús David Cifuentes Pardo 2017

Chapter 1

Abstract

In the last decades the interest in the “search of Majorana fermions” in condensed matter systems [1] has increased due to their potential applications in quantum computing. As recently as 2012, experimental works reporting the detection of such quasiparticles [2, 3]. Later works [4, 5, 6, 7], including a recent paper published by the advisor of this dissertation and collaborators [8], set out to explore the interplay of such Majorana zero-modes with strongly interacting systems such as semiconductor quantum dots, which can be readily integrated in the device. This research project aims to expand this idea using the numerical renormalization group to study the model of a double quantum dot coupled to metallic leads and to a topological superconductor supporting edge Majorana zero modes. This simple model allows the manipulation of the majorana modes bringing possible applications to braiding procedures . In addition, we will study the interplay of Kondo correlations, exchange interactions and Majorana physics.

Chapter 2

Table of Contents

1 Abstract	2
2 Table of Contents	3
3 Motivation	6
3.1 Structure	8
4 Preliminaries	9
4.1 Transport in Quantum Dots (QDs)	9
4.2 The Anderson Model	11
4.3 Kondo Effect	13
4.3.1 Kondo Effect in QDs	14
5 Theory and Methods	15
5.1 Ballistic transport	15
5.1.1 Solving transport equations with graphs	16
5.1.2 Graph Algorithm	18
5.1.3 Ballistic transport in a Double Quantum Dot	19
5.2 The Numerical Renormalization Group (NRG)	22
5.2.1 Density Matrix Renormalization Group (DM-NRG)	29
5.2.2 NRG results in a Double Quantum Dot	29
6 The Pursuit of Majorana Fermions	31
6.1 The Kitaev Chain	31
6.1.1 Topological phase transition	33
6.2 Real implementations of Majorana Chains	36
6.3 Coupling Majoranas to QDs	37
6.3.1 Non-interacting QD coupled to a Majorana chain	38
6.3.2 NRG: Kondo-Majorana physics	40
7 Coupling Majorana Mode to a Double Quantum Dot	41
7.0.1 a) Removing Kondo and Majorana with QD-interference	44
7.0.2 b) Indirect Majorana after Removing Kondo with QD-interference	45

7.0.3 e) Transferring the MZM through gate voltage shifting ϵ_2 .	47
7.1 Particle-Hole symmetric shifting of $\epsilon_2 = \frac{U}{2}$.	50
7.2 Shifting t_2	51
References	52
Bibliography	52

Appendices

A Appendix	56
A.1 Proof of the Graph Method for Transport Equations.	56
B Three peak appearance in the Double Quantum Dot model.	57
B.1 Initial DQD-Majorana Hamiltonian.	58

List of Abbreviations

The next list describes several abbreviations that will be later used within the body of the document

DOS Density of States

DQD Double Quantum Dot

MBS Majorana Bound State

QD Quantum Dot

Chapter 3

Motivation

In 2001 Alexei Yu. Kitaev presented a model for implementing qubits that could face the problem of high decoherence in quantum computation [1]. Kitaev's idea was centered in using the properties of an exotic quasi-particle that appears at the edges of a quantum superconducting chain. This quasi-particle receives the name of Majorana Fermion, is characterized for being its own anti-particle, thus it has no charge or spin. It also presents non-Abelian statistics, a desired property to implement fault-tolerant quantum computers[9]. These majorana fermions were theoretically predicted since the 1930's by one of the genius of the era, Ettore Majorana [10]. Although no fundamental Majorana-particle has been discovered to the date, Kitaev's model inspired the pursue of majorana fermions as quasi-particles in a novel exotic class of materials known as topological superconductors (TS)[11, 12, 3].

The last five years have been full of excitement, as new experiments have turned some of the theoretical predictions of the 1990s and 2000s into a reality. Very recently the first evidence of Majorana end states in TS has been found in multiple experiments [13, 14, 15] following the prescription by Oreg et al. [16] and Lutchyn et al. [17]. These experiments have been based on tunneling spectroscopy in junctions between TS and non metallic (NM) leads, where resonances have been observed at zero energy, consistent with the presence of Majorana zero-energy modes.

A downside of the tunneling spectroscopy technique in this case, is that it probes not only the end of the Topological Superconductor(TS), but its bulk as well , which completely destroys the qubit information. A less destroying model presented by Liu and Baranger [4] consists consists in attaching a Quantum Dot (QD) to the edges of a majorana chain in the topological phase and executing transport measurements through the QD [4] . The majorana mode at the end of the chain then leaks inside the QD [6] which produces a zero-bias conductance peak of half a quanta $\frac{e^2}{2h}$ through the dot. This is a majorana signature which produces half of the expected peak by a regular fermion.

In fact, this phenomenon is similar to the $\frac{e^2}{h}$ conductance peak caused by the Kondo effect [18]. Since topological superconductors and the Kondo effect could coexist at temperatures of a few mili-kelvins, it should be possible to observe combined Kondo-Majorana physics in this type of devices. This idea motivated an NRG study of a Quantum dot-Majorana hibrid system in the Kondo regime [8].

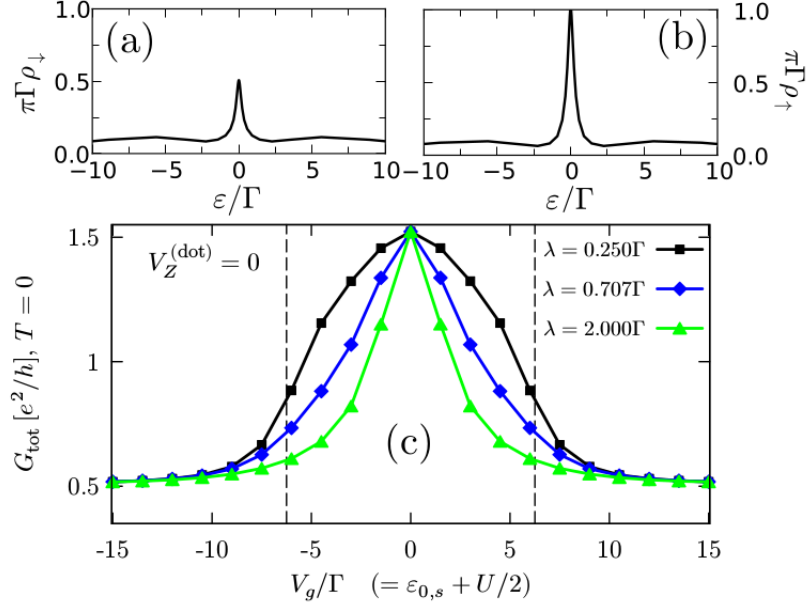


Figure 3.1: (a) QD spin-down density of states. Because this channel couples to the Majorana mode, it displays the characteristic zero-bias signature of amplitude $\frac{e^2}{2h}$. (b) QD spin-up density of states, displaying the zero-bias peak of the Kondo effect, with unit amplitude. (c) Zero-bias conductance of the QD coupled to the Majorana mode, as a function of the QD energy level (λ parameterizes the strength of the Majorana-QD tunnel coupling). The presence of the spin-up Kondo resonance enhances the QD conductance in particle-hole symmetry ($V_g = 0$), but quickly disappears as the QD level is detuned from this point. The spin-down Majorana signature, on the other hand, is robust [7], leaving a residual conductance of $\frac{e^2}{2h}$.

Source: [8].

This study revealed that transport measurements through the quantum dot will show contributions to the enhanced conductance coming from the Kondo effect and the Majorana mode: The Majorana mode at the end of the wire will migrate into one of the quantum dot spin channels, giving rise to a zero-energy peak in the density of states (Figure 3.1a)) contributing a conductance of $\frac{e^2}{2h}$ (Figure 3.1c)). The zero-bias peak from the Kondo effect appears in the other spin channel (Figure 3.1b)), contributing a conductance of $\frac{e^2}{h}$. Then, the Kondo effect can be “turned off” through gate voltages and magnetic fields, leaving only the Majorana contribution. Clear evidence of the destruction of the Kondo peak will appear in the conductance, allowing for a distinction between Majorana and Kondo signatures.

Apart from not destroying the entire qubit-information the QD-method has another insight. This is the possibility of manipulating Majorana fermions in multidot systems by shifting the QD gate voltages and tunnel couplings which brings possible applications in braiding procedures. The simplest system where Majorana manipulation is possible is a Double Quantum Dot (DQD) coupled to a majorana chain. By tuning the QD gate voltages and the majorana coupling we will be able to probe the mobility of the majorana modes through the dots.

In addition, when both dots are coupled to the lead the Double Quantum Dot exhibits an anti-ferromagnetic interaction known as Ruderman-Kittel-Kasuya-Yosida (RKKY) [19, 20, 21]. On the other hand, when only one dot is coupled and the second Dot is indirectly attached through the first dot, the Kondo effect is annihilated due to the destructive interference generated by extra dot [22]. Both cases reveal interesting results for majorana manipulation and hybrid Kondo-Majorana systems.

3.1 Structure

This thesis is integrated by 4-major chapters . In chapter 4, we will take a review to the basis of quantum transport in single electron transistors, the Anderson model and the emergence of the Kondo effect in quantum dots.

In chapter 5 contains a description of the methods that we will use to study the Double Quantum Dot-majorana system. The methods are the Zubarev's ballistic transport[23] for non-interacting systems and Wilson's Numerical Renormalization Group (NRG) technique [24] for interacting systems. We will use the Double Quantum Dot case as major example to explain both methods. Hence the background information about double quantum dots systems will be presented in this chapter.

The chapter 6 changes the subject, leading us to the mean topic of this thesis, Majorana fermions. The discussion will start with the Kitaev chain addressing its main characteristics such as topological characterization and non-abelian statistics . Then we take a look to the real implementations of majorana chains were we will discuss the most recent experimental accomplishments in the area. At the end, we face the the problem of a hybrid Quantum Dot-Majorana system using the methods described in chapter 5.

Using the methods from chapter 5 and the previous acquired experience with the Double Quantum Dot and the Quantum Dot-Majorana , we address in chapter 7 the Double Quantum Dot-Majorana system. We will study several procedures mainly focused in the manipulation of majorana fermions and the combined effects of Kondo-Majorana physics.

Chapter 4

Preliminaries

We will start with a description of transport processes in QDs which will lead us to talk about the Anderson model. Then we will take a look to the Kondo effect and, in particular, to its consequences in quantum dots.

4.1 Transport in Quantum Dots (QDs)

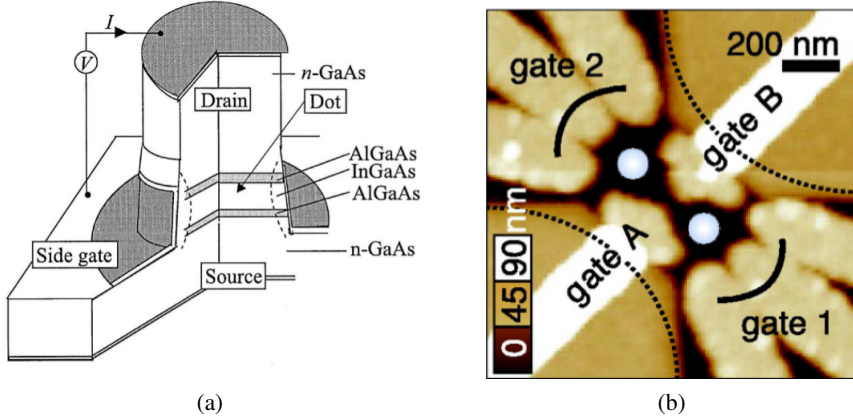


Figure 4.1: a) Vertical quantum dot. b) Atomic force microscopy picture of two coupled lateral QDs (bright central circles). Gates 1 and 2 act as drain and source voltage. A negative voltage is applied at gates A,B to allow the formation of the droplets inside the free space in the 2D electron gas.

Source: [25]

Quantum mechanical effects are visible when the system size is of the order of the de Broglie wavelength [26, (1.1)]

$$\lambda_f = \frac{h}{\sqrt{3m_{\text{eff}}k_B T}}$$

where m_{eff} is the electron effective mass in the crystal. Since m_{eff} can be much smaller than the free electron mass in some semiconducting materials, size quantization effects can be observed at system of sizes $\sim 100\text{nm}$ [27, 2.1]. A device confined in the three dimensions up to

4.1. Transport in Quantum Dots (QDs)

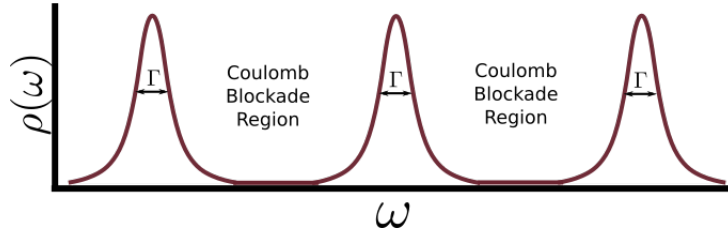


Figure 4.2: Pictorial representation of the Density of States of a QD. The gate potential V_G can be tuned to change the fermi energy of the dot.

Source: *By the author*

this length-scale will present the behavior of a 0D quantum system, which is what we call a Quantum Dot (QD).

Nowadays, QDs can be manufactured with several methods, forms and orientations [26]. According to their orientation with respect to the based 2D-plane , two main types of QDs can be distinguished : Vertical (Figure 4.1a) and lateral (Figure 4.1b) QDs. Both types of of quantum dots have 3-main gates. Two of them are the Drain V_D and source V_S gate voltages used to control the current trough the QD. The third one is the gate voltage V_G . This one controls the electron confinement inside the QD. Therefore, tuning the gate voltage it is possible to control accurately the energy levels of the QD.

Ideally, the energy spectrum of a QD is a discrete set of energy levels resembling the spectrum of an atom. However, when the QD is connected to metallic leads these energy levels hybridized with respect to a hybridization parameter Γ which depends on the voltage connecting the lead with the dots V as

$$\Gamma \propto \pi \|V\|^2 \quad (4.1)$$

in a flat band. A representation of this fact can be found in Figure 4.2. Ideally, $\Gamma \ll \Delta E$ such that the energy levels do not overlap each other. In addition the gate voltage allows us to tune the energy levels of the QD.

To execute transport measurements the QD must be attached to two leads (See 4.3a). Each lead will have a characteristic gate voltage V_S (Left lead) and V_D (Right lead). An electron can pass from the source to the drain if there is an energy level in the middle of the two voltages, just as in 4.3a. However if this condition is not satisfied the dot enters into a coulomb blockade region without electron transport between both leads as can be observed in 4.3b. Inside the coulomb blockade regions the number of electrons is constant. When increasing V_G a single electron enters into the dot each time. Since all of these effects can be controlled by a tuning the gate voltage, the system described is indeed a single electron transistor (SET).

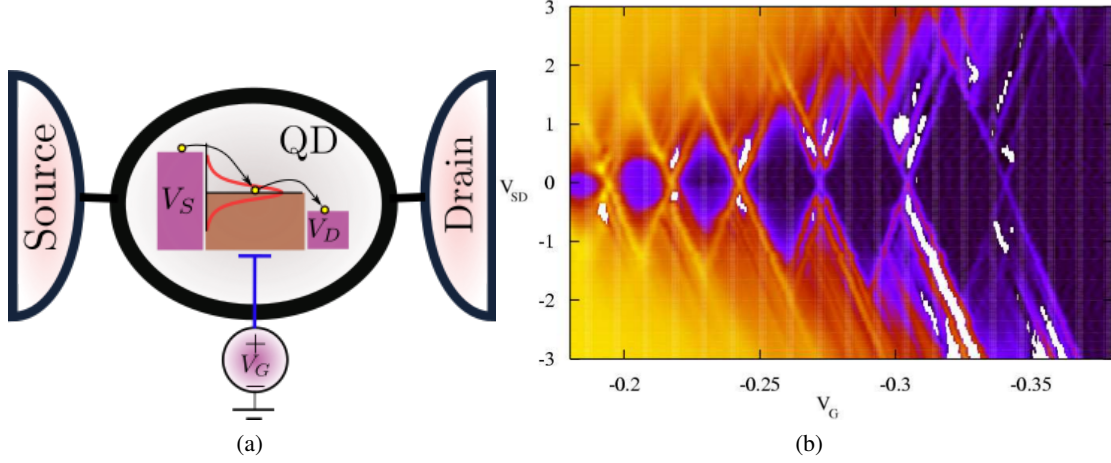


Figure 4.3: a) Representation of transport through QD. The red curve represents the hybridized energy level. The gate voltage tunes this level. In the case represented, the energy level is in the middle of the drain and source voltages allowing transport between the leads. Charging diagram of a quantum dot. b) Plot of the conductance vs the gate voltage V_G and the source-drain voltage ($V_{SD} = V_S - V_D$)

Source: a) By the Author , b) [27]

4.2 The Anderson Model

The Anderson model [28] was originally designed to study the physics of magnetic impurities, which makes it a perfect model to study the Kondo Effect that we will describe in the following section. However, QDs also behave like magnetic impurities. Hence the physics of QDs can be studied using the Anderson model.

Moreover, there are two regimes that will be particularly important in this thesis. They depend on whether Coulomb repulsion is important or not. These are

- **Non-interacting systems:** This means the coulomb repulsion is not relevant . In this case, spin- \uparrow and spin- \downarrow channels are independent which simplifies many of the procedures. The method used to describe solve this systems is ballistic transport.
- **Interacting systems:** The coulomb repulsion is relevant. The repulsion factor will be defined by the factor U . In this case, the spin- \uparrow and spin- \downarrow channels are not independent since the coulomb repulsion limits the number of particles inside each dot. We will use the Numerical Renormalization Group to treat this kind of systems.

The Anderson model takes in account both regimes and the only difference in each case will be the value of U parameter ($U = 0$ non-interacting , $U > 0$ interacting). Taking this in account we proceed to present the Anderson model in QDs.

4.2. The Anderson Model

Using the Hunds rules we know that the energy levels inside the dot should be filled from lower to higher energies with two electrons with different spin at each state. Each pair of electrons will interact magnetically and electrically. In addition, there is an energy associated to each electron and a Zeeman splitting factor in case a \hat{z} -directed magnetic field B is placed. Considering these interactions we can obtain a very general expression in second quantization for the QD Hamiltonian of the form [27, (3.2)]

$$H_d = \sum_{i\sigma} \varepsilon_{di} d_{i\sigma}^\dagger d_{i\sigma} + \sum_i U_i \hat{n}_{i\uparrow} \hat{n}_{i\downarrow} + \sum_{\sigma\sigma', i \neq j} U_{ij} \hat{n}_{i\sigma} \hat{n}_{j\sigma'} - \mu_B g B \sum_i S_i^z + J \sum_{i \neq j} \mathbf{S}_i \cdot \mathbf{S}_j.$$

Where $\sigma \in \{\uparrow, \downarrow\}$, $d_{i\sigma}^\dagger (d_{i\sigma})$ is the dot creation(annihilation) operator, $\hat{n}_{i\sigma} := d_{i\sigma}^\dagger d_{i\sigma}$ is the particle number, \mathbf{S}_i is the spin-vector, ε_{di} is the energy of the i^{th} -level in the dot, U_i is the coulomb repulsion between electrons in the same energy level i , U_{ij} is the coulomb interaction between electrons in different levels (And therefore smaller than U_i), B is an applied magnetic field in the \hat{z} -direction and J is the term representing the Zeeman splitting.

At low temperatures, the main interactions only with the level closest to the Fermi energy. This allows us to make the single-level approximation, neglecting the other energy levels. This assumption reduces the complexity of the dot Hamiltonian to

$$H_d = \sum_{\sigma} \varepsilon_{dd} d_{\sigma}^\dagger d_{\sigma} + U \hat{n}_{\uparrow} \hat{n}_{\downarrow} - \mu_B g B S^z. \quad (4.2)$$

The lead hamiltonian is decomposed in two hamiltonians. The energy of the electrons inside the leads H_{lead} and the interaction between the leads and the quantum dot H_{int} . These hamiltonians take the form

$$\begin{aligned} H_{lead} &= \sum_{\mathbf{k}\sigma l} \varepsilon_{\mathbf{k}l} c_{\mathbf{k}\sigma l}^\dagger c_{\mathbf{k}\sigma l} \\ H_{int} &= \sum_{\mathbf{k}\sigma l} V_{\mathbf{k}l} c_{\mathbf{k}\sigma l}^\dagger d_{\sigma} + V_{\mathbf{k}l}^* d_{\sigma}^\dagger c_{\mathbf{k}\sigma l}, \end{aligned}$$

where \mathbf{k} represents the possible crystal momentums in the leads, $l \in \{S, D\}$, $c_{\mathbf{k}\sigma l}^\dagger (c_{\mathbf{k}\sigma l})$ creates(annihilates) an electron with momentum \mathbf{k} and spin σ in the lead l , $\varepsilon_{\mathbf{k}l}$ is the energy of the electron in the leads and $V_{\mathbf{k}l}$ is a hopping exchange term between the leads and the QD.

In conclusion the sum of these three interactions is receives the name of Anderson Model.

$$\begin{aligned} H &= H_d + H_{lead} + H_{int} \\ &= \sum_{\sigma} \varepsilon_{dd} d_{\sigma}^\dagger d_{\sigma} + U \hat{n}_{\uparrow} \hat{n}_{\downarrow} - \mu_B g B S^z + \sum_{\mathbf{k}\sigma l} \varepsilon_{\mathbf{k}l} c_{\mathbf{k}\sigma l}^\dagger c_{\mathbf{k}\sigma l} + \sum_{\mathbf{k}\sigma l} V_{\mathbf{k}l} c_{\mathbf{k}\sigma l}^\dagger d_{\sigma} + V_{\mathbf{k}l}^* d_{\sigma}^\dagger c_{\mathbf{k}\sigma l}. \quad (4.3) \end{aligned}$$

For this project, we will make two extra changes to the Anderson model. Using the anti-commutation properties of the fermion operators

$$\{d_\sigma^\dagger, d_{\sigma'}\} = \delta_{\sigma\sigma'}, \{d_\sigma^\dagger, d_{\sigma'}^\dagger\} = \{d_\sigma, d_{\sigma'}\} = 0$$

we get

$$\begin{aligned} (d_\uparrow^\dagger d_\uparrow + d_\downarrow^\dagger d_\downarrow - 1)^2 &= \sum_\sigma (d_\sigma^\dagger d_\sigma)^2 - 2 \sum_\sigma d_\sigma^\dagger d_\sigma + 2 d_\uparrow^\dagger d_\uparrow d_\downarrow^\dagger d_\downarrow - 1 \\ &= 2 d_\uparrow^\dagger d_\uparrow d_\downarrow^\dagger d_\downarrow - \sum_\sigma d_\sigma^\dagger d_\sigma - 1. \end{aligned}$$

Replacing this in (4.2) we obtain a nice spin-symmetric form of the dot hamiltonian

$$\left(\varepsilon_d + \frac{U}{2}\right) d_\sigma^\dagger d_\sigma + \frac{U}{2} (d_\sigma^\dagger d_\sigma - 1)^2 - \mu_B g B S^z. \quad (4.4)$$

In addition, it is possible to do a linear transform to the lead operators

$$\frac{1}{\sqrt{V_S^2 + V_R^2}} \begin{bmatrix} V_S & V_R \\ -V_R & V_S \end{bmatrix} \begin{bmatrix} c_{\mathbf{k}\sigma S} \\ c_{\mathbf{k}\sigma D} \end{bmatrix} = \begin{bmatrix} c_{\mathbf{k}\sigma+} \\ c_{\mathbf{k}\sigma-} \end{bmatrix} \quad (4.5)$$

After the transformation the operator will be decoupled from the dot hamiltonian $c_{\mathbf{k}\sigma-}$. This implies that we can suppose that the **dot is coupled with just one lead**. During the rest of the thesis we will maintain this convention.

4.3 Kondo Effect

Note Here goes a review about the Kondo Effect. I am still trying to figure out how it section will look like. For now I'm just leaving some ideas and plots.

In the early 30s the physicist were intrigued by the observation of a resistance minimum in some metals at low temperatures ($\sim 10K$) [27]. The phenomenon received the name of Kondo effect [18]. This effect is attributed to the electron-scattering with the magnetic impurities present in the materials.

Using perturbation theory is possible to explain how this spin flip produces a temperature dependent effect which introduces an additional logarithmic term to the resistivity of the form

$$\rho_{Kondo}(T) \propto \ln\left(\frac{T_{kondo}}{T}\right), \quad (4.6)$$

which occurs due to the spin-flip between the particles in the impurity and in the reservoir. The entire resistivity including and

We can see that under the scale of temperature defined by T_k the Kondo effect dominates over all other interactions. However, there is a fundamental problem in the Kondo model. For

temperatures much smaller than T_K the resistivity diverges. This problem is solved by applying a re-normalization group approach to treat the strong correlations appearing at low temperatures. In the Kondo problem a logarithmic discretization is used. The numerical procedure receives the name of Numerical renormalization Group (NRG).

4.3.1 Kondo Effect in QDs

The problem of magnetic impurities in metals can be treated using the Anderson model in a similar form as the transport in quantum dots. Hence, it is not a surprise that Kondo Effect could also occur in QDs. When an odd number of electrons is in the QD the last level bellow the Fermi energy is half-occupied and hence the dot is magnetized. The unlocalized electrons in the reservoirs then interact with this localized electron . Spin-flip can occur as in the case of magnetic impurities in metals. At low temperatures, this magnetic interaction gives rise to strong quantum correlations that favor the formation of a singlet state between the localized electron and the electrons in the leads. As a result, the zero-bias density of states is increased producing a zero-bias conductance peak.

Note that the physical implications of the Kondo effect between the case of magnetic impurities in metals and transport through QD are different. The reason for this is difference in the dimension in both processes . While the scattering at 3D systems against magnetic impurities should produce a drop in the conductivity at low temperatures, the scattering in 0D systems enhances the conductivity of the QD due to the few scattering directions. This implies that the Kondo Effect in QDs acts in the opposite way as in the impurity case.

Chapter 5

Theory and Methods

5.1 Ballistic transport

The Green function G of a Hamiltonian H is the operator that satisfies the homogenous equation

$$\left(i\hbar \frac{\partial}{\partial t} - H\right)G(t-t') = \delta(t-t'). \quad (5.1)$$

This type of differential equations are solved taking the Fourier transform

$$G_H(\omega) = \int_{-\infty}^{\infty} G(t-t') e^{i\omega(t-t')/\hbar} \delta(t-t') \quad (5.2)$$

In this new space the solution of the equation is

$$(\omega + is - H)G_\omega(\omega) = I.$$

The term $+is$ in the previous hamiltonian is part of a mathematical trick quite common in this theory. During the whole procedure, the Green function acts on the complex field. But when we need to obtain a physical interpretation we will take the limit $s \rightarrow 0$ to obtain the result for real energies. The next step is to decompose $G_H(\omega)$ in the eigenbase of the Hamiltonian $\{|\alpha\rangle\}$ by

$$G_{\alpha,\alpha'}(\omega) = \langle \alpha | G_H(\omega) | \alpha' \rangle = \frac{\delta_{\alpha\alpha'}}{\omega - is - \varepsilon_\alpha} = \frac{\delta_{\alpha\alpha'}(\omega + is - \varepsilon_\alpha)}{(\omega - \varepsilon_\alpha)^2 + s^2}. \quad (5.3)$$

From the famous formula

$$\lim_{s \rightarrow 0} \frac{s}{(\omega - \varepsilon_\alpha)^2 + s^2} = \pi \delta(\omega - \varepsilon_\alpha) \quad (5.4)$$

we obtain

$$Im[G_{\alpha,\alpha'}(\omega)] = \pi \delta(\omega - \varepsilon_\alpha) \delta_{\alpha,\alpha'}. \quad (5.5)$$

Note that the sum of $Im[G_{\alpha,\alpha}(\omega)]$ over all the eigenstates of H is simply the π times the Density of States:

$$\rho(\omega) = -\frac{1}{\pi} Im[G_{\alpha,\alpha}(\omega)^\dagger]. \quad (5.6)$$

An extended definition of the Green function can be given in terms of fermionic operators in second quantization. The time-green function for two fermionic operators A and B is

$$G_{A,B}(t-t') = \mathcal{T}[\{A(t), B(t')\}]. \quad (5.7)$$

Here, causality is important, which is the reason why we use the time-order operator \mathcal{T} . Again, it is possible to define the green-functions in the energy space applying a Fourier transform. The evolution of these Green functions will be determined by the Schrodinger equation. At the end, the result will be

The equation above receives the name of transport equation. This will be our leading method to compute the green functions of the system. In addition we can define the Density of States associated to an operator A to be

$$\rho_{A,A^\dagger} = -\frac{1}{\pi} \text{Im} [G_{A,A^\dagger}(\omega)]. \quad (5.8)$$

This density of states contains important physical information related to operator A . In our case, operator A^\dagger will be related to the creation operator of a quantum dot d^\dagger . Our main purpose will be to compute the density of states of a quantum dot ρ_{d,d^\dagger} . This that allows us to obtain other transport

5.1.1 Solving transport equations with graphs

Solving the transport equations involves dealing with a set of linear equations where all the possible variables including ω , and the Hamiltonian parameters are assumed to be constant. This can be done by Gauss-Jordan elimination, noting that after each elimination process we need to carry on the account in terms of these variables. The solution will be a polynomial fraction with the variable given by these parameters. When the number of operators in the Hamiltonian increases the number of terms in the polynomial grows-up exponentially. This reveals the importance of exploring new methods that could simplify the solution.

The method presented here uses graph theory algorithms that provide a shortcut to Gauss-Jordan elimination [29]. To probe this method we solve here the transport equations for a non-interacting ($U = 0$) DQD connected to one lead. According to the Anderson model the Hamiltonian for this system looks like

$$H = t_{dots} d_1^\dagger d_2 + t_{dots}^* d_2^\dagger d_1 + \sum_{i=1}^2 \epsilon_{di} d_i^\dagger d_i + \sum_k (V_i d_i^\dagger c_{\mathbf{k}} + V_i^* c_{\mathbf{k}}^\dagger d_i) + \epsilon_{\mathbf{k}} c_{\mathbf{k}}^\dagger c_{\mathbf{k}}. \quad (5.9)$$

Since the system is non-interacting we ignore the spin-degeneracy of this Hamiltonian. The only new parameter here is the term t_{dots} , which represents the tunneling between both quantum dots. Using equation (??) with $B = d_1^\dagger$ and A shifting among other operators we compute the

5.1. Ballistic transport

following transport equations

$$(\omega - \varepsilon_1) G_{d_1, d_1^\dagger}(\omega) = 1 + t_{dots} G_{d_2, d_1^\dagger}(\omega) + V_1^* \sum_{\mathbf{k}} G_{c_{\mathbf{k}}, d_1^\dagger}(\omega) \quad (5.10)$$

$$(\omega - \varepsilon_k) G_{c_{\mathbf{k}}, d_1^\dagger}(\omega) = V_1 G_{d_1, d_1^\dagger}(\omega) + V_2 G_{d_2, d_1^\dagger}(\omega) \quad (5.11)$$

$$(\omega - \varepsilon_2) G_{d_2, d_1^\dagger}(\omega) = t_{dots} G_{d_1, d_1^\dagger}(\omega) + V_2^* \sum_{\mathbf{k}} G_{c_{\mathbf{k}}, d_1^\dagger}(\omega) \quad (5.12)$$

This system is already closed which means that we don't need any other equation to find the solution. The matrix form takes the form

$$\begin{bmatrix} \omega - \varepsilon_2 & -V_2 & -t_{dots} \\ -V_2^* & \omega - \varepsilon_k & -V_1 \\ -t_{dots}^* & -V_1^* & \omega - \varepsilon_1 \end{bmatrix} \begin{bmatrix} G_{c_{\mathbf{k}}, d_1^\dagger}(\omega) \\ G_{d_2, d_1^\dagger}(\omega) \\ G_{d_1, d_1^\dagger}(\omega) \end{bmatrix} = \begin{bmatrix} 0 \\ 0 \\ 1 \end{bmatrix} \quad (5.13)$$

By convenience we changed the order of the rows in the matrix. Although this matrix is not Laplacian, the procedure in [29] can still be applied with the downside of loosing some of the speed-up advantages of the algorithm. Still, some advantages of graphs are preserved. From these we point out the possibility of taking minimal cuttings and the relation between these graphs and random walks in the graph. Both advantages simplify the complexity of the solution.

Now, our objective is to compute the green function $G_{d_{1\downarrow}, d_{1\downarrow}^\dagger}(\omega)$. For this we take the graph $\mathcal{G}_{d_1 d_2}$ associated to the matrix in (5.13). The result is observed in Figure 5.1.a). The vertexes of this graph will be the operators in the first site of the of the green functions $(d_{1\downarrow}, d_2, c_k, d_1^\dagger)$. d_1^\dagger is not included since it only appears in the second sub-index of the green functions. The edges are given by the non-diagonal sites in the matrix. In addition, an energy parameter is assigned to each vertex, according to the corresponding term in the diagonal. These energies can also be taken as edges connecting each vertex with itself.

The algorithm consists in the following. Each step of Gauss-Jordan elimination leads to a new graph with different energies and couplings. The elimination of a row and column is equivalent to pop-out the corresponding vertex in the graph. For instance, lets eliminate the first row and column of the matrix in (5.13). For it we just need to subtract the rank-1 matrix with the same first row and first column.

$$\begin{bmatrix} \omega - \varepsilon_k & -V_2 & -V_1 \\ -V_2^* & \omega - \varepsilon_2 & -t_{dots} \\ -V_1^* & -t_{dots}^* & \omega - \varepsilon_1 \end{bmatrix} - \begin{bmatrix} \omega - \varepsilon_k & -V_2 & -V_1 \\ -V_2^* & \frac{V_2^* V_2}{\omega - \varepsilon_k} & \frac{V_2^* V_1}{\omega - \varepsilon_k} \\ -V_1^* & \frac{V_2 V_1^*}{\omega - \varepsilon_k} & \frac{V_1^* V_1}{\omega - \varepsilon_k} \end{bmatrix} = \begin{bmatrix} 0 & 0 & 0 \\ 0 & \omega - \varepsilon_2 - \frac{V_2^* V_2}{\omega - \varepsilon_k} & -t_{dots} - \frac{V_2^* V_1}{\omega - \varepsilon_k} \\ 0 & -t_{dots}^* - \frac{V_2 V_1^*}{\omega - \varepsilon_k} & \omega - \varepsilon_1 - \frac{V_1^* V_1}{\omega - \varepsilon_k} \end{bmatrix} \quad (5.14)$$

The graph associated to this matrix can be observed in Figure 5.1.b). The first vertex corresponding to operator c_k has been popped out. The energies and couplings are modified according to the possible walks passing through the vertex c_k . For instance d_1 's energy ε_1 receives an

5.1. Ballistic transport

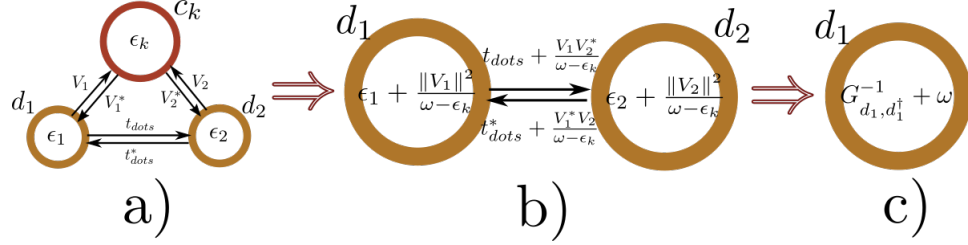


Figure 5.1: a) Graph $\mathcal{G}_{d_1 d_2}$ b) After the elimination of vertex c_k , the energies of dots d_1 and d_2 , and the coupling parameter are changed. c) After Gaussian elimination of dot 2 the energy of dot 1 is the inverse of $G_{d_1, d_1^\dagger}(\omega)$.

Source: *By the author.*

extra-term $\frac{V_1^* V_1}{\omega - \epsilon_k}$ representing an additional walk from d_1 to d_1 passing through c_k . The same logic can be applied to the other terms.

The next stage will turn out into a single vertex as in Figure 5.1.c). As a result of Gauss-Jordan elimination it turns out that the energy of this vertex is the inverse of the green function $G_{d_1 d_1^\dagger}$. The final result is then

$$G_{d_1, d_1^\dagger}(\omega) = \left[\left(\omega - \epsilon_1 - \frac{V_1 V_1^*}{\omega - \epsilon_k} \right) - \frac{\left(t_{dots} + \frac{V_1 V_2^*}{\omega - \epsilon_k} \right) \left(t_{dots} + \frac{V_1 V_2^*}{\omega - \epsilon_k} \right)^*}{\omega - \epsilon_2 - \frac{\Gamma_2^2}{\omega - \epsilon_k}} \right]^{-1}. \quad (5.15)$$

Just one additional correction. Remember that every term including ϵ_k is summing over all possible energies in the momentum space. We avoided this sum during the process to avoid carrying this term during the process. But it is important to include it now.

$$G_{d_1, d_1^\dagger}(\omega) = \left[\left(\omega - \epsilon_1 - \sum_k \frac{V_1 V_1^*}{\omega - \epsilon_k} \right) - \frac{\left(t_{dots} + \sum_k \frac{V_1 V_2^*}{\omega - \epsilon_k} \right) \left(t_{dots} + \sum_k \frac{V_1 V_2^*}{\omega - \epsilon_k} \right)^*}{\omega - \epsilon_2 - \sum_k \frac{\Gamma_2^2}{\omega - \epsilon_k}} \right]^{-1}. \quad (5.16)$$

5.1.2 Graph Algorithm

This is the same procedure we will use in future processes. Just to summarize, the algorithm consists in

1. Compute the transport equations with the second term fixed in the creation operator of the dot you are going to compute the green function.
2. Set up the initial graph.
3. Pop out a vertex:

- (a) Compute the extra-terms in the energies and couplings based on the walks passing through the vertex that will be popped out.
 - (b) Eliminate this vertex from the graph.
 - (c) Iterate till having just one vertex.
4. Invert the last energy to obtain the final green function of the dot.

5.1.3 Ballistic transport in a Double Quantum Dot

The equation (5.16) depends on the factor $\sum_k \frac{V_i^* V_j}{\omega - \epsilon_k}$. This factor describes the broadening of the DOS when the QD enters in contact with the lead. This broadening is usually named $\Gamma_i = V_i^* V_i$ (Or Δ depending on the text book). In general V_i is a function of \mathbf{k} . However, in the limit of flat-band, that is the case we are interested in, we can assume that V_i is constant. Therefore, it is enough to integrate

$$\sum_k \frac{1}{\omega - \epsilon_k + is} = \int_{-D}^D \frac{d\epsilon_k}{\omega - \epsilon_k + is} = -\ln \left(\frac{D - \epsilon_k + is}{-D - \epsilon_k + is} \right) \xrightarrow{D \rightarrow \infty} -i. \quad (5.17)$$

Where we assumed that there is a maximum energy cutoff D going to infinity in the wide-band limit. Hence

$$-i\Gamma_i = \sum_k \frac{V_i^* V_i}{\omega - \epsilon_k}. \quad (5.18)$$

We can replace this in equation (5.15) to obtain the real expression for the green function $G_{d_1, d_1^\dagger}(\omega)$. The terms of the form $V_1 V_2^*$ can be replaced for $\sqrt{\Gamma_1 \Gamma_2}$, supposing there is no additional complex phase.

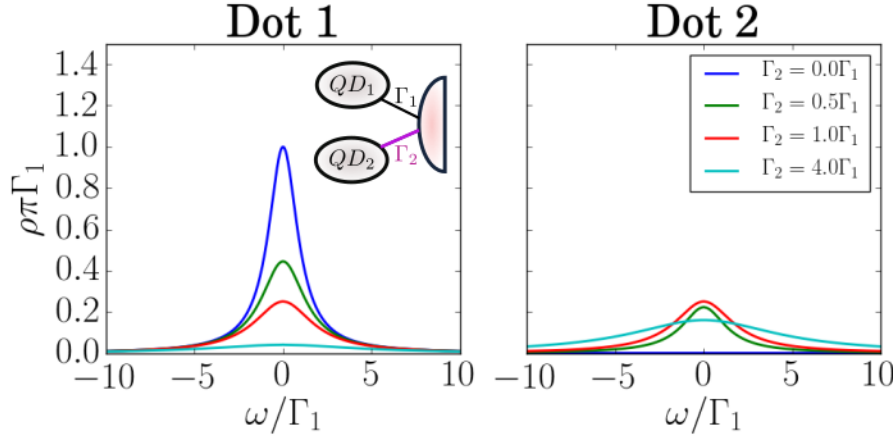
Now, remember from (5.8) that the DOS ρ depends on the imaginary factor of the Green Function $G_{d_1, d_1^\dagger}(\omega)$. This factor is express in the broadening Γ . In case $\Gamma = 0$ the density of states will be null. At any other case, one of the dots should be attached to the lead. Let Γ_1 be the broadening of this dot. We will take Γ_1 as unit. In Figure 5.2 we can observe the evolution of the Density of States under certain processes. Each plot includes an inset showing the model applied to the figure. The coupling in purple indicates the tuning variable. In addition, we set $e_1 = e_2 = 0$ so that both dots satisfy hole symmetric

1. **Coupling QD2 (Figure 5.2a):** It shows the evolution of the DOS when the second dot's coupling scales from 0 to 4Γ . At $\Gamma_2 = 0$ the second dot is decoupled. The first dot's DOS is the same of a single dot case. The maximum height is achieved at $\rho\pi\Gamma_1 = 1$ and the width at the half of this height ($\rho\pi\Gamma_1 = 0.5$) is Γ_1 just as in Figure Figure 4.2. When the second dot is attached $\Gamma_2 > 0$ the density of states is divided between both dots. At $\Gamma_1 = \Gamma_2$ both DOS are equal to $\frac{1}{4\pi\Gamma}$.
2. **Indirect Coupling of QD2 (Figure 5.2b):** This is the most interesting case. When the second dot is connected indirectly through the first dot there appears a quantum inference

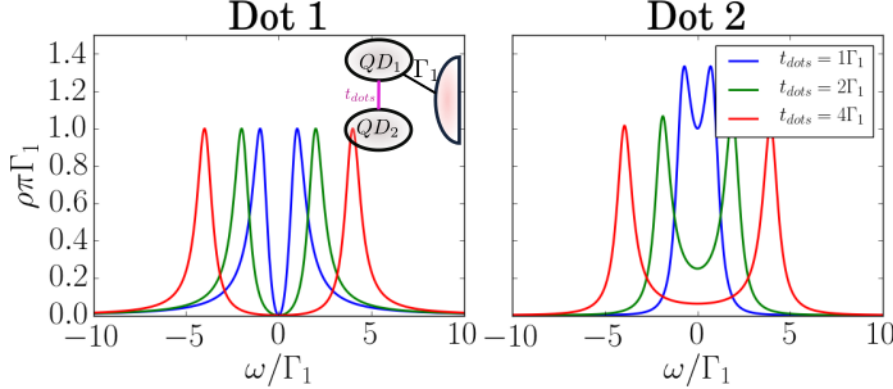
5.1. Ballistic transport

that splits the central peak in two new states. We will observe later that in the interacting case this procedure can also destroy the Kondo signature. This has interesting consequences when combined with majorana physics, since the interference pattern destroy the Kondo effect but not the majorana signature.

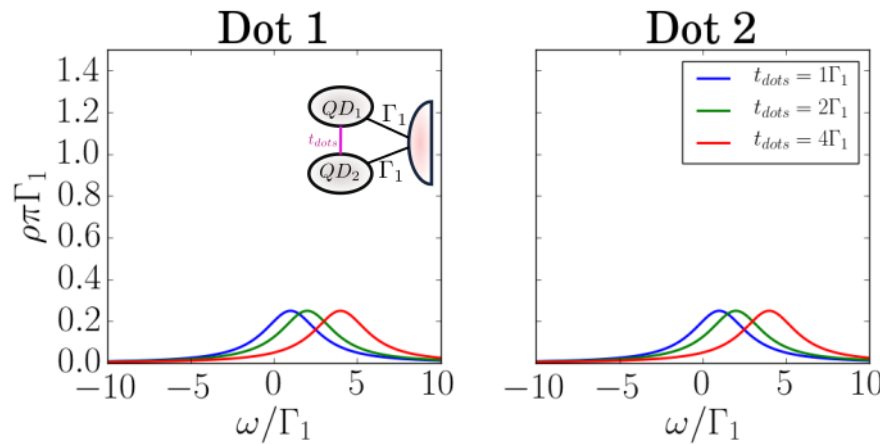
3. **Breaking Particle Hole Symmetry (Figure 5.2c):** Suppose we have $\Gamma_2 = \Gamma_1$. The "triangular connections" break Particle Hole Symmetry. The central peak is displaced to the positive part of the spectrum. Contrary to the previous case, this situation will be avoided during this project. This is because breaking PHS in both dots will prevent the Majorana to tunnel inside the DQD.



(a) Attaching QD2 to the lead



(b) Indirect connection of QD2



(c) Breaking PHS with triangular connection

Figure 5.2: For the tree cases we considered $e_1 = e_2 = 0$. The inset shows the set-up. At each case the purple coupling shows the tuning variable.

Source: *By the Author*

5.2 The Numerical Renormalization Group (NRG)

Note *I need to reference Kondo equations. Include advantages*

At low energies a renormalization group approach is necessary to deal with the effects of high correlations. This implies that the divergent resistivity in Kondo model will be renormalized to a finite quantity.

In the 1970's G.Wilson created a numerical method to solve the Anderson model . This method receives the name of Numerical Renormalization Group (NRG) [? 24, 30]. It consists of three basic steps :

1. To perform a numerical discretization of the energy spectrum in logarithmic intervals.
2. To map the discretized model onto a semi-infinity chain Hamiltonian.
3. To diagonalize iteratively the chain hamiltonian .

The final result will be the spectrum of the Hamiltonian. Other important properties of the material such as density of states, conductivity, specific heat, susceptibility can also be computed. On this project we are mainly interested in the Density of States (DOS). The method used to compute the DOS is the Density Matrix numerical renormalization Group (DM-NRG). A complete description of this algorithm will be given in the followin sections.

For now, we proceed to describe how the NRG is applied to solve the Anderson model in a QD:

Note *I still need to do a long revision to this section. Probably I will send most of the computations to the abstract and leave a summary of NRG and its advantages in the main text.*

Logarithmic Discretization:

We start with an Anderson model hamiltonian such as the one in (4.3) without magnetic field

$$H = \frac{U}{2} + \sum_{\sigma} \left[\left(\varepsilon_d + \frac{U}{2} \right) d_{\sigma}^{\dagger} d_{\sigma} + \frac{U}{2} (d_{\sigma}^{\dagger} d_{\sigma} - 1)^2 + \sum_{\mathbf{k}} \varepsilon_{\mathbf{k}} c_{\mathbf{k}\sigma}^{\dagger} c_{\mathbf{k}\sigma} + V_{\mathbf{k}} d_{\sigma}^{\dagger} c_{\mathbf{k}\sigma} + V_{\mathbf{k}}^* c_{\mathbf{k}\sigma}^{\dagger} d_{\sigma} \right]. \quad (5.19)$$

At low-energies we can assume that QD couples only to s-wave states in the leads[30]. This implies that that the Fermi surface is contained in a single, isotropic conduction band extending inside some fixed cutoffs $-D$ and D . Thus, $\varepsilon_{\mathbf{k}}$ only depends on $|\mathbf{k}|$. This makes possible to

transform the sum over \mathbf{k} in equation 5.19 into an integral over ε between the energy cutoffs

$$H = \sum_{\sigma} \left[\left(\varepsilon_d + \frac{U}{2} \right) d_{\sigma}^{\dagger} d_{\sigma} + \frac{U}{2} (d_{\sigma}^{\dagger} d_{\sigma} - 1)^2 + \int_{-D}^{D} d\varepsilon \, \varepsilon c_{\varepsilon\sigma}^{\dagger} c_{\varepsilon\sigma} \right. \\ \left. + \int_{-D}^{D} \sqrt{\rho_{\sigma}(\varepsilon)} d\varepsilon \, V_{\varepsilon} d_{\sigma}^{\dagger} c_{k\sigma} + V_{\varepsilon}^* c_{\varepsilon\sigma}^{\dagger} d_{\sigma} \right]. \quad (5.20)$$

Here $c_{\varepsilon\sigma}^{\dagger}$ creates an electron with energy ε and $\rho_{\sigma}(\varepsilon)$ is the density of states of the system per spin, which appears in the integral due to the change of variable from \mathbf{k} to $\varepsilon \propto |\mathbf{k}|^2$. Finally, we ignore the energy dependence of ρ and V_d and we replace them by their values in the Fermi energy (This approximation has no great relevance which is justified in [30]) and we renormalize the energy band doing the replacements $k = \frac{\varepsilon}{D}$ and $c_{k\sigma} := \sqrt{D} c_{\varepsilon\sigma}$ so that (5.20) becomes

$$H = D \sum_{\sigma} \left[\frac{1}{D} \left(\varepsilon_d + \frac{U}{2} \right) d_{\sigma}^{\dagger} d_{\sigma} + \frac{U}{2D} (d_{\sigma}^{\dagger} d_{\sigma} - 1)^2 + \int_{-1}^{1} dk \, k c_{k\sigma}^{\dagger} c_{k\sigma} \right. \\ \left. + \sqrt{\frac{\Gamma}{\pi D}} \int_{-1}^{1} dk \, d_{\sigma}^{\dagger} c_{k\sigma} + c_{k\sigma}^{\dagger} d_{\sigma} \right] \quad (5.21)$$

$$= H_d + D \sum_{\sigma} \left[\int_{-1}^{1} dk \, k c_{k\sigma}^{\dagger} c_{k\sigma} + \sqrt{\frac{\Gamma}{\pi D}} \int_{-1}^{1} dk \, d_{\sigma}^{\dagger} c_{k\sigma} + c_{k\sigma}^{\dagger} d_{\sigma} \right], \quad (5.22)$$

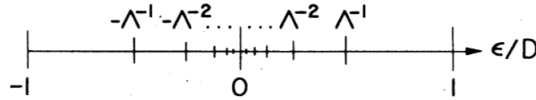


Figure 5.3: Taken from [30]. Energy interval discretization.

where $\Gamma = \pi\rho V^2$ is associated to the lever-width [27, (3.5)]. At this point we have our model dependent of three unit-less constants $\frac{\varepsilon_d}{D}$, $\frac{U}{2D}$ and $\frac{\Gamma}{\pi D}$. The logarithmic discretization starts by defining an scaling parameter $\Lambda \geq 1$ in diving the energy domain $[-1, 1]$ into an array of intervals of the form $\{[\pm\Lambda^{-(n+1)}, \pm\Lambda^n]\}_{n \in \mathbb{N}}$, as we can observe in Figure 5.3. Note that the width of these intervals is decreasing exponentially by

$$d_n = \Lambda^{-n} (1 - \Lambda^{-1}).$$

5.2. The Numerical Renormalization Group (NRG)

Then inside of these energy intervals we can define a set of orthonormal Fourier series of the form

$$\phi_{np}^{\pm}(\varepsilon) = \begin{cases} \frac{1}{\sqrt{d_n}} e^{\pm i \omega_n p \varepsilon} & \varepsilon \in [\pm \Lambda^{-(n+1)}, \pm \Lambda^n] \\ 0 & \text{a.o.c.} \end{cases} \quad (5.23)$$

with $\omega_n := \frac{2\pi}{d_n}$ so that $\phi_{np}^{\pm}(\pm \Lambda^{-(n+1)}) = \phi_{np}^{\pm}(\pm \Lambda^{-n})$. Then we can decompose the creation operators c_k^\dagger into their interval-Fourier contributions as

$$c_{k\sigma}^\dagger = \sum_{np} \phi_{np}^+(k) c_{np\sigma}^{+\dagger} + \phi_{np}^-(k) c_{np\sigma}^{-\dagger} \quad (5.24)$$

with the new creation operators defined as

$$c_{np\sigma}^{\pm\dagger} := (c_{np\sigma}^{\pm})^\dagger = \int_{-1}^1 d\varepsilon [\phi_{np}^{\pm}(\varepsilon)]^* c_{\varepsilon\sigma}^\dagger.$$

This decomposition (5.24) is a simple consequence of the orthonormality of the functions defined in (5.23). In addition we can readily proof that $c_{np\sigma}^{\pm\dagger}$ -operators satisfy the anti-commutation relations, so that they are rightful fermionic creation operators.

We can now use (5.24) to replace the k -dependent terms in hamiltonian (5.21). Then we obtain

$$\begin{aligned} \int_{-1}^1 dk c_{k\sigma}^\dagger d\sigma &= \int_{-1}^1 dk \left(\sum_{np} \phi_{np}^+(k) c_{np\sigma}^{+\dagger} + \phi_{np}^-(k) c_{np\sigma}^{-\dagger} \right) d\sigma \\ &= \left(\sum_{np} \left(\int_{-1}^1 dk \phi_{np}^+(k) \right) c_{np\sigma}^{+\dagger} + \left(\int_{-1}^1 dk \phi_{np}^-(k) \right) c_{np\sigma}^{-\dagger} \right) d\sigma \\ &= \left(\sum_{np} \left(\int_{\Lambda^{-(n+1)}}^{\Lambda^{-n}} dk \frac{e^{i \omega_n p k}}{\sqrt{d_n}} \right) c_{np\sigma}^{+\dagger} + \left(\int_{-\Lambda^{-n}}^{-\Lambda^{-(n+1)}} dk \frac{e^{-i \omega_n p k}}{\sqrt{d_n}} \right) c_{np\sigma}^{-\dagger} \right) d\sigma \\ &= \left(\sum_{np} \sqrt{d_n} \delta_p c_{np\sigma}^{+\dagger} + \sqrt{d_n} \delta_p c_{np\sigma}^{-\dagger} \right) d\sigma \\ &= \sqrt{1 - \Lambda^{-1}} \sum_n \Lambda^{-\frac{n}{2}} (c_{np\sigma}^{+\dagger} + c_{np\sigma}^{-\dagger}) d\sigma. \end{aligned} \quad (5.25)$$

And

$$\begin{aligned}
 \int_{-1}^1 dk k c_{k\sigma}^\dagger c_{k\sigma} &= \sum_{n,n',p,p'} \sum_{s,s'=\pm} \left(\int_{-1}^1 k dk \phi_{np}^s(k) \left(\phi_{np}^{s'}(k) \right)^* \right) c_{np\sigma}^{s\dagger} c_{n'p'\sigma}^{s'} \\
 &= \sum_{n,n',p,p'} \sum_{s,s'=\pm} \left(\frac{\delta_{nn'} \delta_{ss'}}{d_n} \int_{\Lambda^{-(n+1)}}^{\Lambda^{-n}} k dk e^{is\omega_n k(p-p')} \right) c_{np\sigma}^{s\dagger} c_{n'p'\sigma}^s \\
 &= \sum_{npp'} \sum_{s=\pm} \left(\frac{s}{2} \Lambda^{-2n} (1 - \Lambda^{-2}) \delta_{pp'} + \frac{1 - \delta_{pp'}}{is\omega_n(p-p')} \left[ke^{is\omega_n k(p-p')} \right]_{\Lambda^{-(n+1)}}^{\Lambda^{-n}} \right) \frac{c_{np\sigma}^{s\dagger} c_{n'p'\sigma}^{s'}}{d_n} \\
 &= \frac{1}{2} (1 + \Lambda^{-1}) \sum_{np} \Lambda^{-n} (c_{np\sigma}^{+\dagger} c_{np\sigma}^+ - c_{np\sigma}^{-\dagger} c_{np\sigma}^-) \\
 &\quad + \sum_n \sum_{p \neq p'} \frac{1 - \Lambda^{-1}}{2i\pi(p' - p)} (c_{np\sigma}^{+\dagger} c_{n'p'\sigma}^+ - c_{np'\sigma}^{-\dagger} c_{n'p\sigma}^-) e^{\frac{2i\pi(p-p')}{1-\Lambda^{-1}}}. \tag{5.26}
 \end{aligned}$$

Thus, if we replace (5.25) and (5.26) into (5.21) we will obtain a logarithmic discretization of the hamiltonian. The next part will we to map this discretization to an iterative process that is worth for a numerical computations.

Mapping the Anderson model to a Chain-Hamiltonian

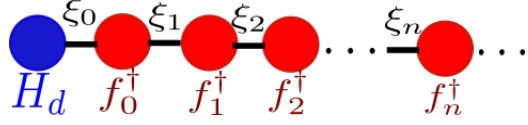


Figure 5.4: Chain-Hamiltonian describing the Anderson model. The chain starts at the initial dot hamiltonian H_d . The f_m^\dagger 's are the creation operators at the n^{th} -site of the chain. The ξ_n 's describe the magnitude of the interaction between consecutive sites.

We are looking for a model just like the one we have in Figure 5.4. This is because a Chain-Hamiltonian will give an iterative approximation of the Anderson model with an increasing (but still controllable) number of degrees of freedom. This will provide the rightful structure for a numerical diagonalization of the hamiltonian.

To do this, observe from equations (5.25),(5.26) that the QD (d_σ) couples directly only to the operators with $p = 0$ ($c_{n0\sigma}^{\pm\dagger}$). The $p \neq 0$ terms will appear in the hamiltonian only because they are coupled to $c_{np\sigma}^{\pm\dagger}$ in Equation (5.26). Thus, as a first approximation we can neglect all terms in (5.26) with $p \neq 0$. This leaves only the first part of (5.26), so that we can define $c_{n\sigma}^{\pm\dagger} := c_{np\sigma}^{\pm\dagger}$. Let

$$f_{0\sigma}^\dagger = \sqrt{\frac{1 - \Lambda^{-1}}{2}} \sum_n \Lambda^{-\frac{n}{2}} (c_{n\sigma}^{+\dagger} + c_{n\sigma}^{-\dagger}), \text{ so that } \sqrt{2} f_{0\sigma}^\dagger d_\sigma = \int_{-1}^1 dk c_{k\sigma}^\dagger d_\sigma. \tag{5.27}$$

5.2. The Numerical Renormalization Group (NRG)

Note $\{f_{0\sigma}^\dagger, f_{0\sigma}\} = \frac{1-\Lambda^{-1}}{2} \sum_n 2\Lambda^{-n} = 1$. Replacing this in (5.21) we get

$$H = H_d + D \sum_\sigma \left[\sqrt{\frac{2\Gamma}{\pi D}} (d_\sigma^\dagger f_{0\sigma} + f_{0\sigma}^\dagger d_\sigma) + \frac{1}{2} (1 + \Lambda^{-1}) \sum_n \Lambda^{-n} (c_{n\sigma}^{+\dagger} c_{n\sigma}^+ - c_{n\sigma}^{-\dagger} c_{n\sigma}^-) \right].$$

f_0^\dagger will represent the first site of the chain-hamiltonian in Figure 5.4 since no other term is coupled to the dot hamiltonian. We also have the coupling term $\xi_0 = \sqrt{\frac{2\Gamma}{\pi D}}$. It is possible to obtain the following f_m^\dagger -operators by supposing a solution of the form

$$f_{m\sigma}^\dagger = \sum_n a_{mn}^+ c_{n\sigma}^{+\dagger} + a_{mn}^- c_{n\sigma}^{-\dagger} = \sum_n \sum_{s=\pm} a_{mn}^s c_{n\sigma}^{s\dagger}, \quad (5.28)$$

such that they satisfy the anti-commutation relations

$$\{f_{m\sigma}^\dagger, f_{m'\sigma'}\} = \delta_{mm'} \delta_{\sigma\sigma'}, \quad \{f_{m\sigma}^\dagger, f_{m\sigma}^\dagger\} = \{f_{m\sigma}^\dagger, f_{m\sigma}^\dagger\} = 0$$

and

$$\frac{1}{2} (1 + \Lambda^{-1}) \sum_n \Lambda^{-n} (c_{n\sigma}^{+\dagger} c_{n\sigma}^+ - c_{n\sigma}^{-\dagger} c_{n\sigma}^-) = \sum_{m=0}^{\infty} \Lambda^{\frac{-m}{2}} \xi_m (f_{m\sigma}^\dagger f_{m+1,\sigma} + f_{m+1,\sigma}^\dagger f_{m\sigma}). \quad (5.29)$$

It is possible to find a solution for this system using the formula of the right part of equation 5.29. Since the relation is only given between consecutive terms $m, m+1$ and we already have the coefficients for $m=0$ ($a_{0n}^s = \sqrt{\frac{1-\Lambda^{-1}}{2}} \Lambda^{-\frac{n}{2}}$). Then it is possible to determine the upper coefficients in a recursive way starting from $m=0$. Supposing we can obtain the m^{th} -coefficients (a_{mn}^s) and then finding iteratively the coefficients of $m+1$ ($a_{m+1,n}^s$) using the relation given by equation (5.29). This provides a numerical way for obtaining the f_m^\dagger operators. In fact in our case, where we actually did important assumptions, the problem can be solved analytically obtaining that the final hamiltonian is given by

$$H = H_d + D \sum_\sigma \left[\sqrt{\frac{2\Gamma}{\pi D}} (d_\sigma^\dagger f_{0\sigma} + f_{0\sigma}^\dagger d_\sigma) + \frac{1}{2} (1 + \Lambda^{-1}) \sum_{n=0}^{\infty} \Lambda^{\frac{-n}{2}} \xi_n (f_{n\sigma}^\dagger f_{n+1,\sigma} + f_{n+1,\sigma}^\dagger f_{n\sigma}) \right]. \quad (5.30)$$

with

$$\xi_n = \frac{1 - \Lambda^{-n-1}}{(1 - \Lambda^{-2n-1})^{\frac{1}{2}} (1 - \Lambda^{-2n-3})^{\frac{1}{2}}}.$$

The formal recursive-solution of this problem can be found in [?]. Note that equation (5.30) describes the chain hamiltonian model that we were looking for in Figure 5.4. Note that in the limit when $n \rightarrow \infty$

$$\Lambda^{\frac{-n}{2}} \xi_n \rightarrow \frac{\Lambda^{\frac{-n}{2}} (1 - \Lambda^{-n})}{1 - \Lambda^{-2n}} \sim \frac{\Lambda^{\frac{-n}{2}}}{1 + \Lambda^{-n}},$$

which implies an exponential decaying of the hopping term in the chain.

Iterative Diagonalization in a Single QD process

Now that we have an iterative representation of the Anderson Model Hamiltonian (5.30), lets take a look to how the NRG code would work for a QD. We start with the dot hamiltonian. (Since the D term is always present as a normalizing factor, we are going to avoid this term in future computations and suppose that we are working with unit-less variables ϵ_d , U and $\Gamma' := \sqrt{\frac{2\Gamma}{\pi D}}$).

$$H_d = \frac{1}{D} \left(\epsilon_d + \frac{U}{2} \right) d_\sigma^\dagger d_\sigma + \frac{U}{2D} (d_\sigma^\dagger d_\sigma - 1)^2. \quad (5.31)$$

Now observe that hamiltonian 5.31 already has a diagonal form in the base $\{| \uparrow\downarrow \rangle, | \uparrow \rangle, | \downarrow \rangle, | 0 \rangle\}$

$$H_d = \frac{1}{D} \begin{bmatrix} 2\epsilon_d + \frac{3U}{2} & 0 & 0 & 0 \\ 0 & \epsilon_d + \frac{U}{2} & 0 & 0 \\ 0 & 0 & \epsilon_d + \frac{U}{2} & 0 \\ 0 & 0 & 0 & \frac{U}{2} \end{bmatrix}.$$

Lets define $H_{-1} = \Lambda^{\frac{-1}{2}} H_d$. Adding the first chain interaction to H_d we obtain a new hamiltonian of the form

$$H_0 = \Lambda^{\frac{1}{2}} H_{-1} + \Gamma' (d_\sigma^\dagger f_{0\sigma} + f_{0\sigma}^\dagger d_\sigma). \quad (5.32)$$

The Hilbert space for this hamiltonian has to be extended to include the 4 degrees of freedom of the $f_{0\sigma}^\dagger$ particles which are also given by $\{| \uparrow\downarrow \rangle, | \uparrow \rangle, | \downarrow \rangle, | 0 \rangle\}$. Therefore the total Hilbert space for H_0 is given by a base of the form

$$|s_1\rangle|s_2\rangle := |s_1\rangle \otimes |s_2\rangle \text{ with } |s_{1,2}\rangle \in \{| \uparrow\downarrow \rangle, | \uparrow \rangle, | \downarrow \rangle, | 0 \rangle\}.$$

This gives an space of dimension $4 \times 4 = 16$. Now before adventuring to write the hamiltonian for H_0 as a 16×16 -matrix note that H_0 preserves particle number N and the total spin S . Therefore we can use N and S as quantum numbers and generate the Hamiltonian H_0 in blocks. We will observe that the terms in the diagonal will correspond to the eigenvalues of H_{-1} for the first space. The non-diagonal terms are the result of the hopping interactions with the first site.

$$H_{N=0,S=0} :$$

$$|0\rangle|0\rangle \rightarrow \left[\frac{U}{2} \right]$$

$$H_{N=4,S=0} :$$

$$| \uparrow\downarrow \rangle| \uparrow\downarrow \rangle \rightarrow \left[2\epsilon_d + \frac{3U}{2} \right]$$

$$H_{N=1,S=\frac{1}{2}} :$$

$$\begin{aligned} | \uparrow \rangle| 0 \rangle &\rightarrow \left[\begin{array}{cc} \epsilon_d + \frac{U}{2} & \Gamma' \\ 0 & \Gamma' \end{array} \right] \\ | 0 \rangle| \uparrow \rangle &\rightarrow \left[\begin{array}{cc} \Gamma' & \frac{U}{2} \end{array} \right] \end{aligned}$$

$$H_{N=1,S=\frac{-1}{2}} :$$

$$\begin{aligned} | \uparrow \rangle| 0 \rangle &\rightarrow \left[\begin{array}{cc} \epsilon_d + \frac{U}{2} & \Gamma' \\ \Gamma' & \frac{U}{2} \end{array} \right] \\ | 0 \rangle| \uparrow \rangle &\rightarrow \left[\begin{array}{cc} \Gamma' & \frac{U}{2} \end{array} \right] \end{aligned}$$

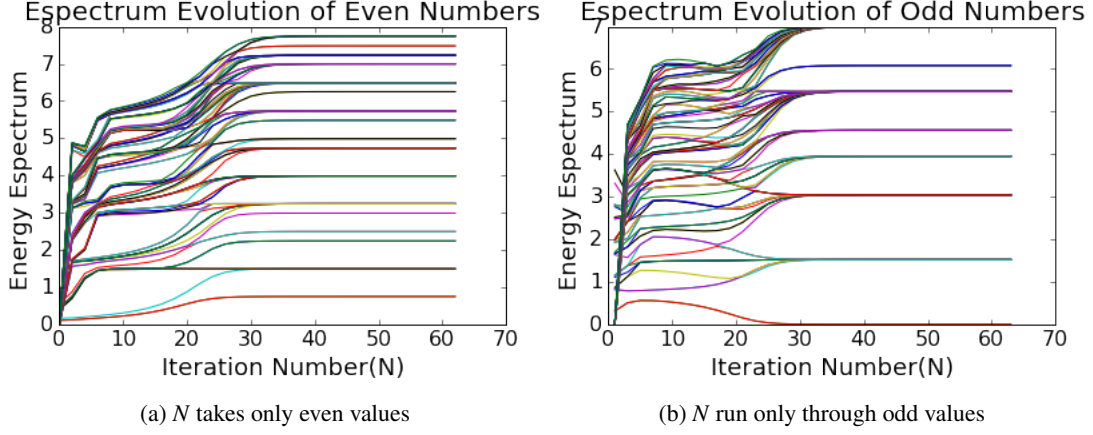


Figure 5.5: Evolution of the QD-spectrum vs number of iterations of the code for $U = 0.5$, $e_d = -0.25$, $\Gamma = 2.82 \times 10^{-2}$.

$H_{N=2,S=-1}$:

$$|\downarrow\rangle|\downarrow\rangle \rightarrow [\varepsilon_d + \frac{U}{2}]$$

$H_{N=2,S=1}$:

$$|\uparrow\rangle|\uparrow\rangle \rightarrow [\varepsilon_d + \frac{U}{2}]$$

$H_{N=2,S=0}$:

$$\begin{aligned} |\uparrow\downarrow\rangle|0\rangle &\rightarrow \left[2\varepsilon_d + \frac{3U}{2}, \Gamma, -\Gamma, 0 \right] \\ |\uparrow\rangle|\downarrow\rangle &\rightarrow \left[\Gamma, \varepsilon_d + \frac{U}{2}, 0, \Gamma \right] \\ |\downarrow\rangle|\uparrow\rangle &\rightarrow \left[-\Gamma, 0, \varepsilon_d + \frac{U}{2}, -\Gamma \right] \\ |0\rangle|\uparrow\downarrow\rangle &\rightarrow \left[0, \Gamma, -\Gamma, \frac{U}{2} \right] \end{aligned}$$

$H_{N=3,S=\frac{1}{2}}$:

$$\begin{aligned} |\uparrow\downarrow\rangle|\uparrow\rangle &\rightarrow \left[\varepsilon_d + \frac{U}{2}, -\Gamma' \right] \\ |\uparrow\rangle|\uparrow\downarrow\rangle &\rightarrow \left[-\Gamma', \frac{U}{2} \right] \end{aligned}$$

$H_{N=3,S=\frac{-1}{2}}$:

$$\begin{aligned} |\uparrow\downarrow\rangle|\downarrow\rangle &\rightarrow \left[\varepsilon_d + \frac{U}{2}, -\Gamma' \right] \\ |\downarrow\rangle|\uparrow\downarrow\rangle &\rightarrow \left[-\Gamma', \frac{U}{2} \right] \end{aligned}$$

Finally, we proceed to diagonalize H_0 by blocks $H_{N,S}$. The resulting eigenvectors will be characterized by both quantum numbers so that we can write them in the form $|N, S, i\rangle$ with i takes as many values as the degeneracy of its block. For higher values of N , the general formula for equation (5.32) looks as

$$H_{N+1} = \Lambda^{\frac{1}{2}} \left[H_N + \frac{1}{2} (1 + \Lambda^{-1}) \xi_N (f_{N\sigma}^\dagger f_{N+1,\sigma} + f_{N+1\sigma}^\dagger f_{N\sigma}) \right]. \quad (5.33)$$

We now proceed by induction supposing that for each N the Hamiltonian H_N is already diagonalized and the eigenvectors are organized in states with labels $|N, S, i\rangle$. The next step will be to add the 4-Hilbert space corresponding to $f_{N+1,\sigma}$ organized the eigenvectors according to the

quantum numbers $|N', S', i\rangle$ and proceed to diagonalize by blocks the new Hamiltonian. Apart of it, the code must have a cutoff to the number of states.

This NRG code was previously implemented in C++ language by the advisor of this thesis. In Figure 5.5 we observe the evolution of the spectrum of the Hamiltonian according to the number of iterations of the code. As we can appreciate, this evolution converges for even and odd number around $N = 30$.

5.2.1 Density Matrix Renormalization Group (DM-NRG)

To compute dynamical quantities [31] like the density of states is the DMNRG [32]. Note *Sill planning this section*

5.2.2 NRG results in a Double Quantum Dot

We ran the NRG code for the DQD with the following set of parameters:

$$U_{1,2} = -2\epsilon_{1,2} = 8.62\Gamma_1$$

Figure 5.6 shows the NRG results for the density of states of QD1 in different states. The three plots show the external Coulomb peaks at $e_1 = \frac{U}{2} \sim 8.62\Gamma_1$, which represent the DOS of the energy levels. In addition Figure 5.6a shows a central peak at the fermi energy. **This is the Kondo Peak.**

Figure 5.6b shows the DOS in the case where the two QDs are symmetrically attached. At low energies, the inset shows the appearance of two satellite peaks representing the Ruderman-Kittel-Kasuya-Yosida (RKKY) interaction. This interaction is explained for this particular case in section Appendix B.

Again, the most interesting case is in Figure 5.6c. The additional interference with the second dot completely destroys the Knondo effect. This effect is observed at energies closed to $t_{dots} = 0.689\Gamma$ and will take its relevance in the last chapter.

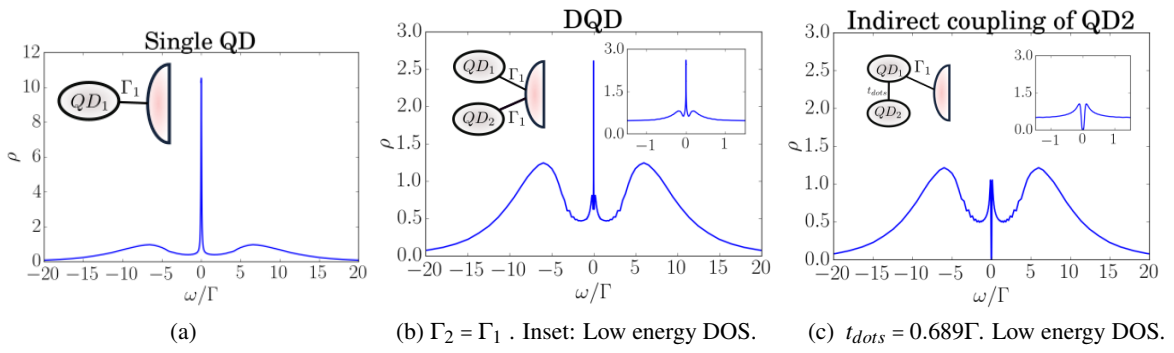


Figure 5.6: Density of states in QD1 predicted by NRG at each case. . The insets show the. Note that figure a) is in a different scale due to a major central peak ..

Source: *By the Author*

Chapter 6

The Pursuit of Majorana Fermions

The Majorana Fermions, so called in the name of the Italian physicist Ettore Majorana, were first defined in the attempt to find a real solution of the Dirac equation. The real field that solves this equation describes a fermion which is its own antiparticle. Hence it has no electric charge nor mass. Till these days, no fundamental particle with these characteristics has been observed. However, in the last decade, there has been a huge speculation about the possibility of finding Majorana Fermions as a quasi-particles of certain types of topological superconductors.

The topological materials are a novel type of material that experiences phase transitions without any symmetry breaking. As consequence, they cannot be characterized by the Landau theory. Instead, the phase transition is characterized with a topological order . Since topological characters are discrete parameters that describe non-local features of the material, the phases with this characterization present robust characteristics that are difficult to alter. An example of this is the quantum hall effect which robustness is famous and widely used in high precision devices.

One of the most promising topological materials is the one dimensional majorana wire. This wire is inspired in a famous Kitaev's toy model representing a spinless p-wave superconducting wire. Under certain conditions, the majorana wires experience topological phase transition characterized by the emergence exotic zero-modes localized at edges of the wire. Kitaev associated these modes with majorana quasi-particles appearing at the boundary of the topological superconducting wire. Moreover, he pointed out that the combined used of robustness from topological materials and Majorana's non-abelian statistics could lead to the creation of fault tolerant quantum gates. This fact opened the doors to the search of majorana fermions in condensed matter physics.

In this chapter we will present a review of the main topics about majorana fermions. In the first section section 6.1, we will describe the the Kitaev's chain and the emergence of majorana zero modes. Next, we will discuss about the real implementations of majorana chains and the experimental proposals that have been carried on . Finally, we will take a look to the results coupling QDs with majorana chains.

6.1 The Kitaev Chain

In this section we discuss the main aspects of Kitaev's toy model. This is a toy model in tight binding that represents a finite p -wave superconducting wire with the following Hamiltonian

$$H = \sum_{i=1}^N [-t(a_i^\dagger a_{i+1} + a_{i+1}^\dagger a_i) - \mu a_i^\dagger a_i + \Delta a_i a_{i+1} + \Delta^* a_{i+1}^\dagger a_i^\dagger]. \quad (6.1)$$

Where μ is the chemical potential, so that $\mu a_i^\dagger a_i$ is the energy associated to each step in the chain. $t(a_i^\dagger a_{i+1} + a_{i+1}^\dagger a_i)$ represents the interaction between neighbouring sites which is determined by the hopping term t . The remaining terms describe the superconducting properties of the system as is established by the BCS theory of superconductivity. Δ is a complex superconducting parameter with the form $\Delta = e^{i\theta} |\Delta|$. The associated terms represent the Cooper pairs which can be created or annihilated at neighbouring sites of the system.

The form of hamiltonian (6.1) favors the possibility of introducing new operators $\gamma_{A,j}$ and $\gamma_{B,j}$ such that

$$\gamma_{A,j} = e^{i\theta/2} a_j + e^{-i\theta/2} a_j^\dagger, \quad \gamma_{B,j} = -i(e^{i\theta/2} a_j - e^{-i\theta/2} a_j^\dagger). \quad (6.2)$$

It is simple check that these operators are self-adjoint ($\gamma_{A,j}^\dagger = \gamma_{A,j}$, $\gamma_{B,j}^\dagger = \gamma_{B,j}$). This is a required constraint for the Majorana particles. In addition they satisfy the fermionic anti-commutation relations

$$\begin{aligned} \{\gamma_{A,i}, \gamma_{A,j}\} &= \{\gamma_{B,i}, \gamma_{B,j}\} = 2\delta_{ij}, \\ \{\gamma_{A,i}, \gamma_{B,j}\} &= 0. \end{aligned} \quad (6.3)$$

This allows us to understand the operators $\gamma_{A,i}, \gamma_{B,i}$ as majorana fermions. If we also take the inverse of (6.2) we obtain that each (Dirac) fermion in Hamiltonian (6.1) is composed by two majorana fermions such that

$$a_j = \frac{e^{-i\theta/2}}{2} (\gamma_{A,j} + i\gamma_{B,j})$$

We could even adventure to say that these majorana operators are actually dividing the Dirac fermions into real(γ_A) and imaginary (γ_B) part ,the same way as complex numbers are a composite of two real numbers.

The new Kitaev Hamiltonian in the Majorana representation looks like

$$H = \frac{i}{2} \sum_{j=1}^N [-\mu \gamma_{A,j} \gamma_{B,j} + (t - |\Delta|) \gamma_{B,j} \gamma_{A,j+1} + (t + |\Delta|) \gamma_{A,j} \gamma_{B,j+1}] + Const, \quad (6.4)$$

Depending on the values of parameters μ, t and $|\Delta|$ we can identify two regimes represented by the following situations:

1. If $|\Delta| = t = 0, \mu < 0$ Hamiltonian (6.4) becomes $\frac{-i\mu}{2} \sum_j \gamma_{A,j} \gamma_{B,j}$ which represents the coupling of the Majoranas in the same Dirac fermion. (See Figure 6.1 (a))
2. If $|\Delta| = t > 0, \mu = 0$ the situation is much more interesting. The Hamiltonian (6.4) takes the form $H = 2ti \sum_j \gamma_{A,j} \gamma_{B,j+1}$. This implies that the coupling is performed between Majoranas of different Dirac fermions leaving the edge Majorana operators ($\gamma_{A,1}$ and $\gamma_{B,N}$) uncoupled

6.1. The Kitaev Chain

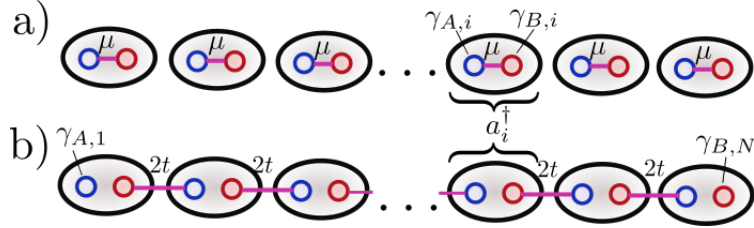


Figure 6.1: Illustration of the Kitaev chain for open boundary conditions in the Majorana representation. a)Represents the trivial case where the hopping and the superconducting term approaches to 0. b) The non-trivial topological phase. The coupling is produced between Majoranas in different Dirac fermions

Source: By the author

(See Figure 6.1b)). Note that these uncoupled majorana fermions can be at any state without any repercussion in the energy of the system. This explains the emergence of a ground state localized at edges of the chain.

These two situations are representatives of two different phases. The trivial phase occurs for $\frac{\mu}{2t} > 1$ and the non-trivial phase appears when $\frac{\mu}{2t} < 1$ (See figure item 6.1). The mean characteristic of the non-trivial phase is the creation of an stable zero-mode. This zero-mode is generated by the uncoupled majorana fermions at the edges of the Kitaev chain.

6.1.1 Topological phase transition

The two regimes described previously can be characterized with a topological parameter. One of the methods for this is following the idea used by Alicea[3]. The first part is to suppose that we have an infinite chain ($N = \infty$) in Hamiltonian (6.4). The new system is translation invariant, hence we can make a transformation to the momentum space. Then we may rewrite Hamiltonian (6.4) as

$$H = \sum_{k \in BZ} \begin{pmatrix} b'_k & c'_k \end{pmatrix} H_k \begin{pmatrix} b'_{-k} \\ c'_{-k} \end{pmatrix}. \quad (6.5)$$

with the Bloch Hamiltonian

$$H_k = \begin{pmatrix} 0 & \frac{-i\mu}{2} + it \cos k + |\Delta| \sin k \\ \frac{i\mu}{2} - it \cos k + |\Delta| \sin k & 0 \end{pmatrix} = (|\Delta| \sin k) \sigma_x + \left(\frac{\mu}{2} - t \cos k \right) \sigma_y. \quad (6.6)$$

where σ_x, σ_y are the corresponding Pauli matrices. The Brilloin zone (BZ) is the periodic space $[-\pi, \pi]$ which can be mapped to the unitary circle. Equation (6.6) determines the coordinates

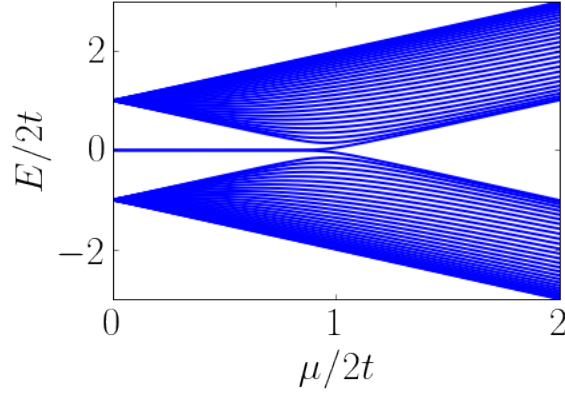


Figure 6.2: Spectrum of Hamiltonian (6.4) with 30 sites and $t = |\Delta|$ s. Method: Numerical diagonalization.

Source: By the author

of the Bloch Hamiltonian in the base $\{\sigma_x, \sigma_y\}$. We can map these coordinates to the unitary circle by taking the norm of this vector giving

$$\hat{H}_k = \frac{1}{\sqrt{|\Delta|^2 \sin^2 k + (\frac{\mu}{2} - t \cos k)^2}} \begin{pmatrix} |\Delta| \sin k \\ \frac{\mu}{2} - t \cos k \end{pmatrix}. \quad (6.7)$$

Note that $|\Delta|^2 \sin^2 k + (\frac{\mu}{2} - t \cos k)^2 \neq 0$ for all the values of k as long as $\frac{\mu}{2t} \neq 1$. When $\frac{\mu}{2t} = 1$ the $H_{k=0} = 0$, so it cannot be normalized. **This is the same point were the phase transition occurs!**. At any other value of $\frac{\mu}{2t}$ it is possible to normalize H_k for all values of $k \in BZ$. The result of mapping \hat{H}_k for all k is a path around the unitary circle.

This path can take two forms as we can observe in Figure 6.1.1. If $\frac{\mu}{2t} > 1$ the path reduced to a line in the upward part of the circle. In the non-trivial phase $\frac{\mu}{2t} < 1$ the path completes the round to the entire circle. Note that this method states a topological difference between the two phases. While the path described by the trivial phase can be contracted to a single dot, the path described by the non-trivial one is a circle that cannot be contracted.

Note that to determine whether path of a given phase is of type a) or type b) we only need to check if $\hat{H}_{k=0}$ and $\hat{H}_{k=\pi}$ are the same point or opposite points. This transforms into a simple equation

$$\hat{H}_{k=0,y} \hat{H}_{k=\pi,y} = \begin{cases} 1 & \text{trivial phase} \\ -1 & \text{non-trivial phase} \end{cases} \quad (6.8)$$

where $\hat{H}_{k=0,y}$ is the y -th component of \hat{H}_k . The term $\hat{H}_{k,y}$ is a particular case of the Pfaffian $\mathcal{P}(k)$, which widely used as topological order in phases transition including majorana modes .

6.1. The Kitaev Chain

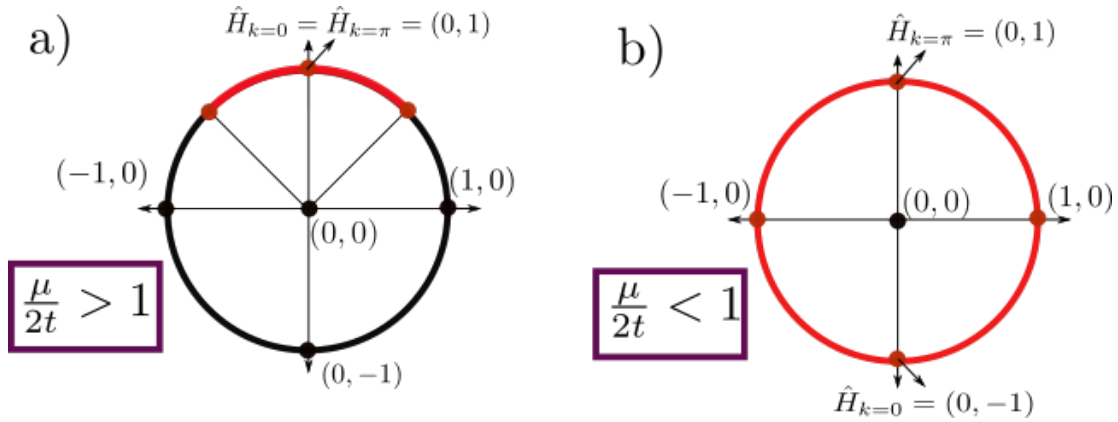


Figure 6.3: The following represents the path of \hat{H}_k for the interval $[-\pi, \pi]$. a) Corresponds to the trivial phase. The resulting path can be homotopically deformed to a point. b) The non-trivial phase corresponds to a non-contractible loop around the unitary circle.

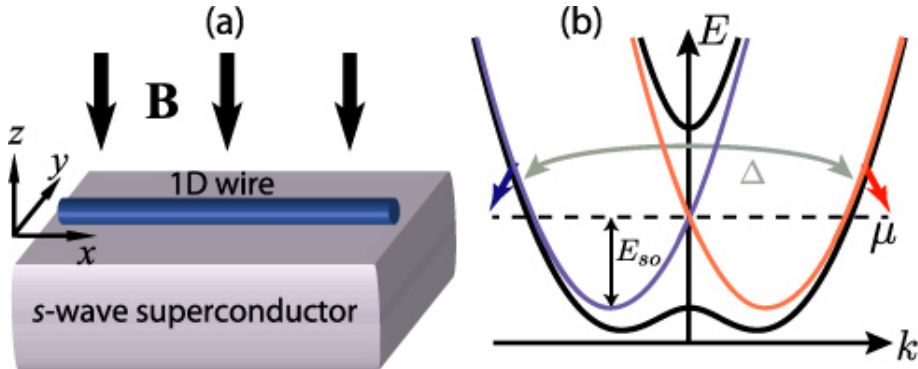
Source: By the author

The mean idea behind this topological characterization relies in the adiabatic theorem. In simple words, the adiabatic theorem says that a slow evolution of a gaped Hamiltonian will produce a smooth evolution of its ordered eigenstates. i.g The order of the eigenstates remains unchanged.

The keyword in the previous definition is "gaped". As we can observe in Figure item 6.1 the phase transition occurs at $\frac{\mu}{2t} = 1$. This is when the system transitions between a gapless and gaped Hamiltonians.

The connection with topology comes from the fact that adiabatic evolutions can be understood as smooth deformations of the Hamiltonian. However since gapless Hamiltonians imply phase transitions, the theory defines the gapless points as holes (or forbidden points) in the phase space. Then characterizing the phase transitions in the Kitaev chain is mainly a topological problem where gaped Hamiltonians are holes in the topological space. In addition, the topological orders characterizing this transition will be Chern or Winding numbers.

Though this connection between physics and topology is quite interesting, I will stop here because it is taking us out of our real discussion which is majorana fermions. You can find more information about this in ([Note](#) [add references](#)).


 Figure 6.4: Source: [3]

6.2 Real implementations of Majorana Chains

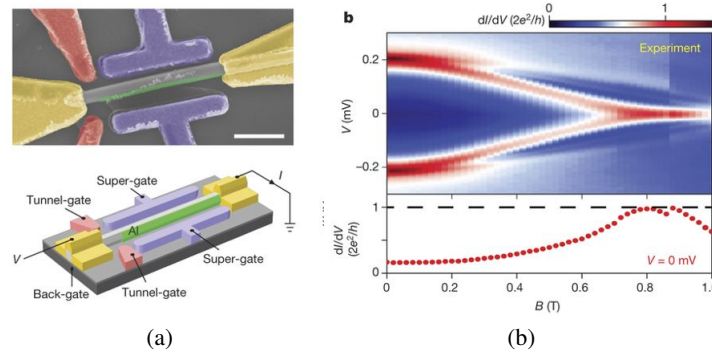
Note Here comes a summary of real models and implementations of majorana chains. I am still thinking how to write this section. For now, I leave some ideas

Although the Kitaev chain its just a toy model, it does describes some interesting physics.

The promise of finding the exotic majorana particles that could bring new insights to quantum computing motivated the implementation of real models that could emulate the physics of a Kitaev chain.

Spin is a major problem. A material with spin-orbit coupling is the solution to this situation.
??

$$H = \int dx \psi^\dagger \left(\frac{\partial^2}{2m\partial x^2} - \mu - i\alpha\sigma_y \partial x + h\sigma_x \right) \psi + \Delta \psi_\downarrow \psi_\uparrow + \Delta^* \psi_\downarrow \psi_\uparrow, \quad (6.9)$$


 Figure 6.5: Source: [33]

6.3 Coupling Majoranas to QDs

Liu and Baranger was one of the first in proposing the possibility of using QDs in the pursuit of Majorana fermions . When a QD is attached to a the end of a majorana chain in the topological phase, the majorana mode at the end of the chain then leaks inside the QD [6]. This produces a zero-bias conductance peak of half a quanta $\frac{e^2}{2h}$ through the dot.

We can reconstruct these results using the methods that we developed in chapter 5. To this lets first define our model hamiltonian:

$$H = H_{QD-Lead} + H_{M-QD} + H_M. \quad (6.10)$$

Where $H_{QD-Lead}$ is the Hamiltonian for the non-interacting Anderson model (4.3), H_M is the Hamiltonian of the majorana chain and H_{M-QD} represents the coupling between the QD and the Majorana Fermion at the boundary.

Now, the real question is how to define the coupling between the QD and the majorana fermion. In fact, there are many ways to represent this interaction. One alternative is to replace in H_M with the entire Kitaev chain hamiltonian (6.1) (or even with the majorana chain (6.9)) and then pick H_{M-QD} as a simple coupling between the QD and the first site of the chain [6]. A simpler approach is to define an effective coupling with the majorana operator at the edge of the majorana chain. Since the Kitaev chain is spin-less, we choose to couple the majorana to the spin- \downarrow channel of the QD ¹. Therefore, the majorana fermion should be the superposition of the creation and annihilation operators of a spin \downarrow particle f_\downarrow :

$$\gamma_1 := \frac{1}{\sqrt{2}} (f_\downarrow^\dagger + f_\downarrow), \gamma_2 := \frac{1}{\sqrt{2}} (f_\downarrow^\dagger - f_\downarrow).$$

This makes possible to define an effective coupling between the Majorana Mode and the dot by attaching γ_1 with the spin- \downarrow channel in the QD

$$H_{M-QD} = t_1 (d_\downarrow^\dagger \gamma_1 + \gamma_1 d_\downarrow) \quad (6.11)$$

Then the coupling with the chain is given by

$$\begin{aligned} H_M &= \epsilon_m f_\downarrow^\dagger f_\downarrow \\ H_{M-QD} &= \frac{t_1}{\sqrt{2}} d_{1\downarrow}^\dagger f_\downarrow + \frac{t_1^*}{\sqrt{2}} f_\downarrow^\dagger d_{1\downarrow} + \frac{t_1}{\sqrt{2}} d_{1\downarrow}^\dagger f_\downarrow^\dagger + \frac{t_1^*}{\sqrt{2}} f_\downarrow d_{1\downarrow} \end{aligned}$$

Finally we obtain the following hamiltonian

¹An appropriate justification of this fact can be found in [8]

$$H = \sum_{k,\sigma} \left(\epsilon_1 + \frac{U_1}{2} \right) d_{1\sigma}^\dagger d_{1\sigma} + \frac{U}{2} (d_{1\sigma}^\dagger d_{1\sigma} - 1)^2 + t_1 (d_{1\downarrow}^\dagger \gamma_1 + \gamma_1 d_{1\downarrow}) + V d_{1\sigma}^\dagger c_{k\sigma} + V^* c_{k\sigma}^\dagger d_{1\sigma} + \epsilon_m f_\downarrow^\dagger f_\downarrow. \quad (6.12)$$

The fidelity of this effective model has been discussed by Ruiz-Tijerina et al. [8] concluding that the majorana effective hamiltonian reproduces the same results than the Kitaev chain model in the topological phase (This statement is true even for more realistic models of the TS that include Rashba spin-orbit interactions and a Zeeman field [8]).

6.3.1 Non-interacting QD coupled to a Majorana chain

In the non-interacting case we can use the ballistic transport equations from section 5.1. The green functions are then determined by the following set of linear equations.

$$(\omega - \epsilon_M) G_{f_\downarrow, d_{1\downarrow}^\dagger}(\omega) = (\omega + \epsilon_M) G_{f_\downarrow^\dagger, d_{1\downarrow}^\dagger}(\omega) = \frac{t_1^*}{\sqrt{2}} \left(G_{d_{1\downarrow}, d_{1\downarrow}^\dagger}(\omega) - G_{d_{1\downarrow}^\dagger, d_{1\downarrow}^\dagger}(\omega) \right) \quad (6.13)$$

$$(\omega - \epsilon_1) G_{d_{1\downarrow}, d_{1\downarrow}^\dagger}(\omega) = 1 + \frac{t_1}{\sqrt{2}} t_1 G_{f_\downarrow, d_{1\downarrow}^\dagger}(\omega) + \frac{t_1}{\sqrt{2}} t_1 G_{f_\downarrow^\dagger, d_{1\downarrow}^\dagger}(\omega) + V_1 \sum_{\mathbf{k}} G_{c_{\mathbf{k}\downarrow}, d_{1\downarrow}^\dagger}(\omega) \quad (6.14)$$

$$(\omega - \epsilon_{\mathbf{k}}) G_{c_{\mathbf{k}}, d_{1\downarrow}^\dagger}(\omega) = V_1^* G_{d_{1\downarrow}, d_{1\downarrow}^\dagger}(\omega) \quad (6.15)$$

$$(\omega + \epsilon_1) G_{d_{1\downarrow}^\dagger, d_{1\downarrow}^\dagger}(\omega) = -\frac{t_1}{\sqrt{2}} G_{f_\downarrow, d_{1\downarrow}^\dagger}(\omega) - \frac{t_1}{\sqrt{2}} G_{f_\downarrow^\dagger, d_{1\downarrow}^\dagger}(\omega) - V_1^* \sum_{\mathbf{k}} G_{c_{\mathbf{k}\downarrow}^\dagger, d_{1\downarrow}^\dagger}(\omega) \quad (6.16)$$

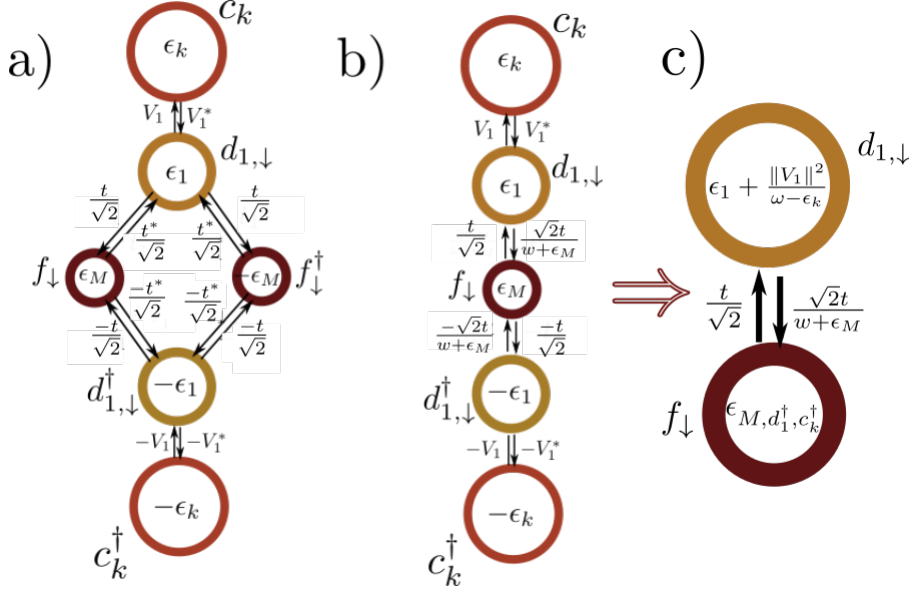
$$(\omega + \epsilon_{\mathbf{k}}) G_{c_{\mathbf{k}}^\dagger, d_{1\downarrow}^\dagger}(\omega) = -V_1^* G_{d_{1\downarrow}, d_{1\downarrow}^\dagger}(\omega) \quad (6.17)$$

The graph representing these green functions is represented in Figure 6.6 a) (Look subsection 5.1.1 for details). However using that $(\omega - \epsilon_M) G_{f_\downarrow, d_{1\downarrow}^\dagger}(\omega) = (\omega + \epsilon_M) G_{f_\downarrow^\dagger, d_{1\downarrow}^\dagger}(\omega)$ we can take $G_{f_\downarrow^\dagger, d_{1\downarrow}^\dagger}(\omega)$ out of the equations getting the system in Figure 6.6 b) . Using the graph algorithm from subsection 5.1.2 we proceed to pop out vertexes c_k , c_k^\dagger and d_1^\dagger in that order. The result is the graph in figure Figure 6.6.c) with

$$\epsilon_{M, d_1^\dagger, c^\dagger} = \epsilon_M + \frac{\omega}{\omega + \epsilon_M} \frac{\|t\|^2}{\omega + \epsilon_1 + \sum_{\mathbf{k}} \frac{V_1 V_1^*}{\omega + \epsilon_{\mathbf{k}}}}. \quad (6.18)$$

We finally pop out f_\downarrow to obtain

$$G_{d_{1\downarrow}, d_{1\downarrow}^\dagger}(\omega) = \left[\omega - \epsilon_1 - \sum_{\mathbf{k}} \frac{V_1 V_1^*}{\omega - \epsilon_1} - \frac{\omega}{\omega + \epsilon_M} \frac{\|t\|^2}{\omega - \epsilon_{M, d_1^\dagger, c^\dagger}} \right]^{-1}. \quad (6.19)$$


 Figure 6.6: Graph \mathcal{G}_M representing the transport equations. Source: By the author

Hence we just need the green function of $G_{f_d, f_d^\dagger}^{\mathcal{G}_M - d_1}(\omega)$ removing d_1 out of the graph. This case is much simpler since f_d is just attached to d_1^\dagger . Thus we get

$$G_{f_d, f_d^\dagger}^{\mathcal{G}_M - d_1}(\omega) = \left[\omega - \varepsilon_M - \frac{\omega}{\omega + \varepsilon_M} \frac{\|t\|^2}{\omega + \varepsilon_1 - \sum_k \frac{V_1 V_1^*}{\omega - \varepsilon_k}} \right]^{-1}. \quad (6.20)$$

Again, the only missing point in this equation is to replace $\sum_k \frac{V_1 V_1^*}{\omega - \varepsilon_k} = -i\Gamma_1$. Note that this computations are only for the spin- \downarrow channel. The spin- \uparrow channel is even simpler since this channel is not coupled to the majorana mode. Hence it corresponds to the case of a single quantum dot coupled to a Lead. The results for the DOS can be observed in Figure 6.7. Each figure has an inset showing the model in the majorana representation. The small blue and red balls are majorana fermions just as the ones in figure 6.1. The majorana at the edge of the majorana chain is represented by the isolated red ball majorana connected to the QD (Figure 6.7a). The other isolated blue ball in Figure 6.7c represents the majorana at the other edge which is connected to the sphere by the parameter ε . Note Here comes the interpretation

Figure: 6.7a

Figure: 6.7b

Figure: 6.7c

6.3. Coupling Majoranas to QDs

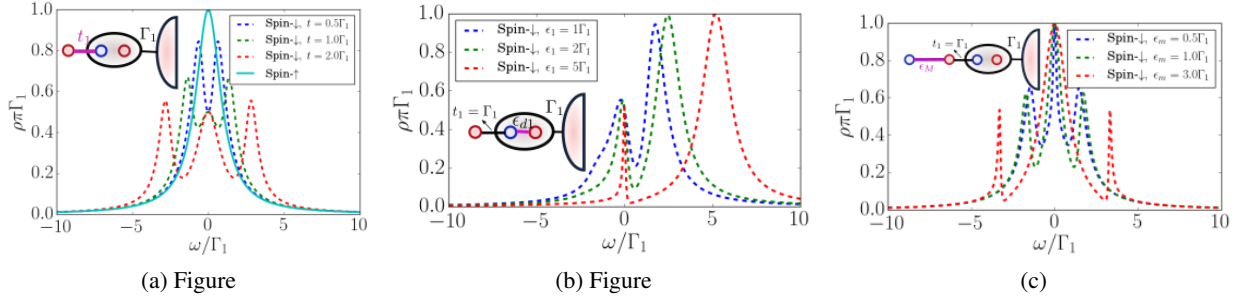


Figure 6.7: Figure .. [Note] I don't like the variables of the c) plot. So I might change them soon.

Source: By the Author

6.3.2 NRG: Kondo-Majorana physics

In the interacting case the Kondo peak will appear at the fermi energy. In addition, the majorana in the spin- \downarrow channel will produce a peak at the fermi energy of Half of the amplitude of the Kondo peak (See Figure 6.8). This will be our majorana signature.

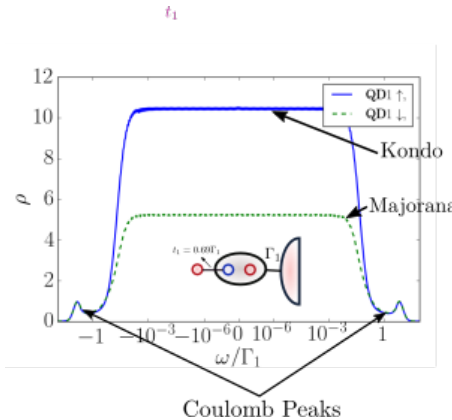


Figure 6.8: [Note] The units of this plot are a bit different than the NRG plots. That's mainly due to a problem I am having with the NRG plots. I will unify the format soon.

Source: [?]

Ruiz-Tijerina et al. proved that this effective coupling is able to reproduce efficiently the results obtained when the Kitaev chain in the topological phase is attached to a single QD.

Chapter 7

Coupling Majorana Mode to a Double Quantum Dot

Note This section is still a bit disorganized since most of the results are new. In this section we present the results for the NRG analysis of the Anderson model applied to the case of a Double Quantum Dot (DQD) attached to a Majorana mode (See Figure 7.1). Extending the Hamiltonian (6.12) to a coupling with a DQD we obtain the following general Hamiltonian:

$$H = \sum_{i=1}^2 \sum_{k,\sigma} \left(\epsilon_i + \frac{U_i}{2} \right) d_{i\sigma}^\dagger d_{i\sigma} + \frac{U_i}{2} (d_{i\sigma}^\dagger d_{i\sigma} - 1)^2 + t_i (\gamma d_{i,\downarrow} + d_{i,\downarrow}^\dagger \gamma) + V_i d_{i\sigma}^\dagger c_{k\sigma} + V_i^* c_{k\sigma}^\dagger d_{i\sigma}. \quad (7.1)$$

Note I neglected ϵ_M in this case. Depending on the future NRG results I will choose to add it or leave it that way.

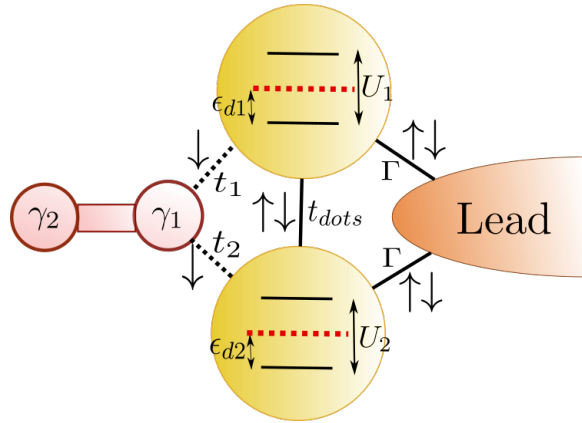


Figure 7.1: General model. Source: By the Author

In order to understand the physical properties of this model, we probed a set of thought processes. The main variable in this analysis is the Density of States. We will observe its evolution on both QDs under the tuning of the model parameters such as the majorana couplings (t_1, t_2), gate voltages (ϵ_1, ϵ_2) and the inter dot coupling (t_{dots})

These processes intend to show whether it is possible to "manipulate" the majorana modes inside the dots by tuning the established parameters. The number of possible combinations of parameters is actually pretty huge. We used ballistic transport tho predict which one of them show interesting physics. Those models where also treated with the NRG approach in the interacting case. The process we selected are summarized in Figure 7.2.

To built the ballistic transport graph (See subsection 5.1.1) we just need to think that our model is actually merging the DQD graph (Figure 5.1) with the Majorana (Figure Figure 6.6.b)). No need to write the green transport equations . Note in graph \mathcal{G}_{MDQD} that the green function $G_{d_{1\downarrow},d_{1\downarrow}^\dagger}(\omega)\mathcal{G}_{MDQD}$ is composed by the greeen function of the DQD $\left(G_{d_{1\downarrow},d_{1\downarrow}^\dagger}^{\mathcal{G}_{d_1d_2}}(\omega)\right)$ and the extra term added by the presence of the majorana opperator f_\downarrow . In the equations this is simply

$$G_{d_{1\downarrow},d_{1\downarrow}^\dagger}^{\mathcal{G}_{MDQD}}(\omega) = \left[\left(G_{d_{1\downarrow},d_{1\downarrow}^\dagger}^{\mathcal{G}_{d_1d_2}}(\omega) \right)^{-1} + \frac{\omega}{\omega + \varepsilon_M} \frac{E_{d_{1\downarrow}f_\downarrow}^{\mathcal{G}_{MDQD}}}{\left[G_{f_\downarrow,f_\downarrow}^{\mathcal{G}_{MDQD-d_1}}(\omega) \right]^{-1}} \right]^{-1}. \quad (7.2)$$

where

$$E_{d_{1\downarrow}f_\downarrow}^{\mathcal{G}_{MDQD}} = \left(t_1 + t_2 \frac{\left(t_{dots} + \sum_{\mathbf{k}} \frac{V_1 V_2^*}{\omega - \varepsilon_{\mathbf{k}}} \right)}{\omega - \varepsilon_2 - \sum_{\mathbf{k}} \frac{V_2 V_2^*}{\omega - \varepsilon_{\mathbf{k}}}} \right) \left(t_1^* + t_2^* \frac{\left(t_{dots}^* + \sum_{\mathbf{k}} \frac{V_1^* V_2}{\omega - \varepsilon_{\mathbf{k}}} \right)}{\omega - \varepsilon_2 - \sum_{\mathbf{k}} \frac{V_2^* V_2}{\omega - \varepsilon_{\mathbf{k}}}} \right). \quad (7.3)$$

Note This fact is difficult to explain. I will need more plots and writing the appendix. For now I will leave here some results

We then need to compute $G_{f_\downarrow,f_\downarrow}^{\mathcal{G}_{MDQD-d_1}}(\omega)$. This graph is much simple. The neighborhood of f_\downarrow in graph \mathcal{G}_{MDQD-d_1} are d_2 (above) and the inverted DQD(bellow). These neighbors are disconnected, hence we can include the in the green function independently. The term above is simply the dot $d_{2\downarrow}$ connected with the lead .

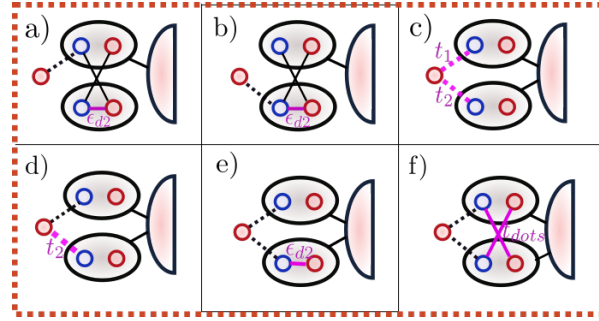
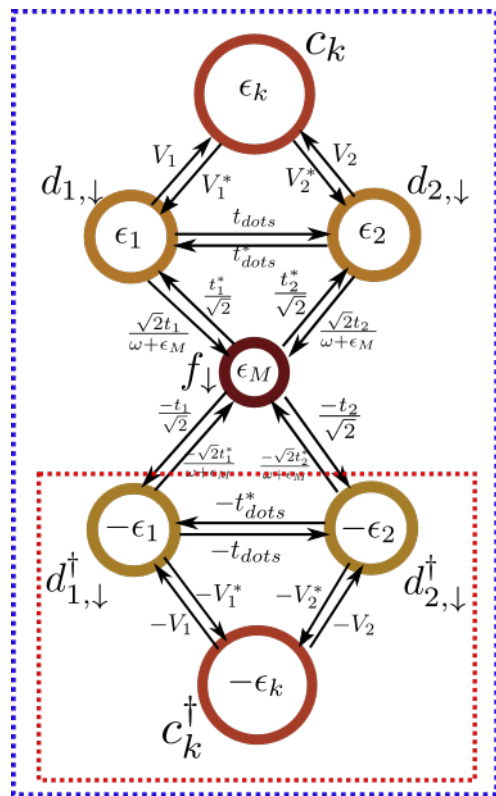
$$\frac{\frac{\omega}{\omega + \varepsilon_M} \|t_2\|^2}{\omega - \varepsilon_2 - \sum_{\mathbf{k}} \frac{V_2 V_2^*}{\omega - \varepsilon_{\mathbf{k}}}}. \quad (7.4)$$

The term generated by the connection of f_\downarrow with the inverted DQD is a bit more complicated. First we need to include the term given by the connection with $d_{2\downarrow}^\dagger$ which is

The other term is the contact with the DQD which can be expressed as

$$G_{f_\downarrow,f_\downarrow}^{\mathcal{G}_{MDQD-d_1}}(\omega) = \left[\omega - \varepsilon_M - \frac{\frac{\omega}{\omega + \varepsilon_M} \|t_2\|^2}{\omega - \varepsilon_2 - \sum_{\mathbf{k}} \frac{V_2 V_2^*}{\omega - \varepsilon_{\mathbf{k}}}} - \frac{\frac{\omega}{\omega + \varepsilon_M} \|t_2\|^2}{\omega + \varepsilon_2 - \sum_{\mathbf{k}} \frac{V_2 V_2^*}{\omega + \varepsilon_{\mathbf{k}}}} - \frac{\omega}{\omega + \varepsilon_M} \frac{E_{f_\downarrow d_{1\downarrow}^\dagger}^{\mathcal{G}_{MDQD-d_1}}}{\left[G_{d_{1\downarrow}^\dagger, d_{1\downarrow}^\dagger}^{\mathcal{G}_{MDQD-d_1-f_\downarrow}}(\omega) \right]^{-1}} \right]^{-1}. \quad (7.5)$$

Now, note that that graph $\mathcal{G}_{MDQD-d_1-f_\downarrow}$ is actually a double quantum dot with negated couplings. Hence $G_{d_{1\downarrow}^\dagger, d_{1\downarrow}^\dagger}^{\mathcal{G}_{MDQD-d_1-f_\downarrow}}(\omega)$ satisfies the equation (5.15) but with variables $-t_{dots}, -t_1, -t_2, -\varepsilon_1, -\varepsilon_2$


 Figure 7.2: Selected Models . Source: By the Author

 Figure 7.3: Graph \mathcal{G}_{MQD} representing ballistic transport through a DQD coupled to a Majorana mode.

Source: By the Author

7.0.1 a) Removing Kondo and Majorana with QD-interference

Note Text coming soon

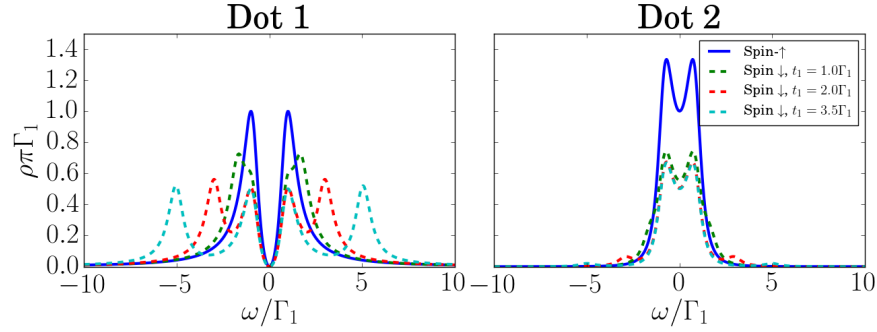


Figure 7.4: Source: By the Author

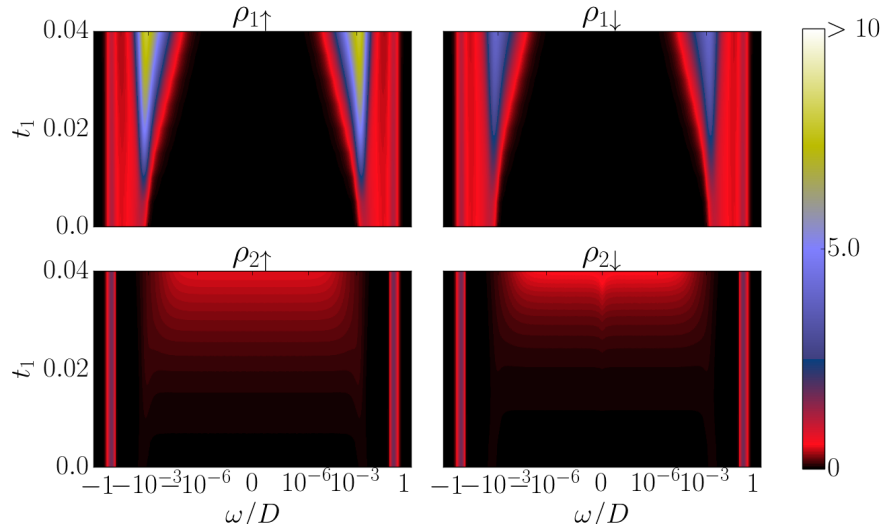


Figure 7.5: Source: By the Author

7.0.2 b) Indirect Majorana after Removing Kondo with QD-interference

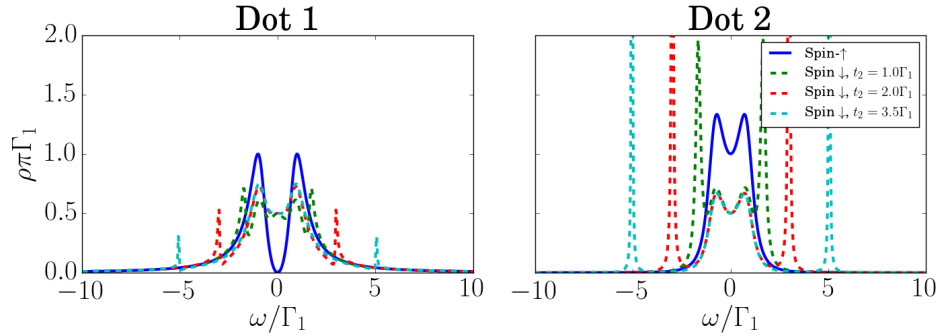


Figure 7.6: Source: By the Author

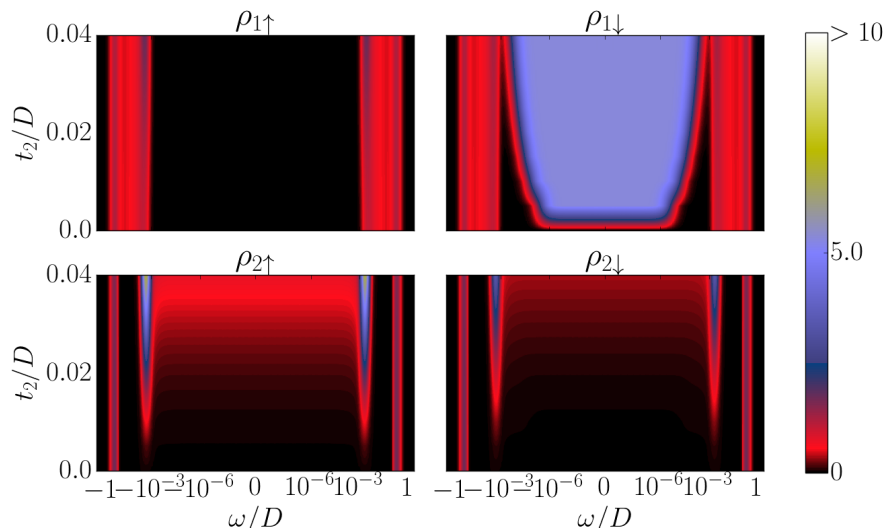


Figure 7.7: Source: By the Author

c) Attaching the Majorana mode to the DQD (Tuning $t_1 = t_2$)

Parameters:

$$\Gamma \sim 2.83 * 10^{-2} D, t_{dots} = 0, U_{1,2} = -2\epsilon_{1,2} = 0.5$$

$$t_1 = t_2 \in [0, 2.5 * 10^{-2} D]$$

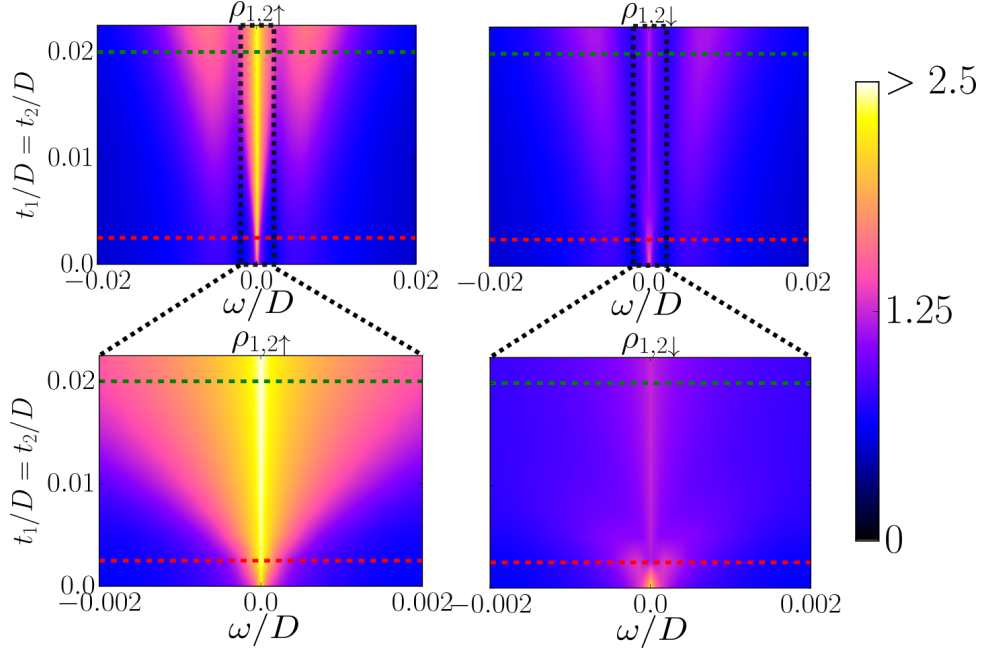


Figure 7.8: Evolution of the DOS of both QDs through $t_1 = t_2$ tuning. UP: Energy scale $\omega \sim 10^{-2} D$. DOWN: Energy scale $\omega \sim 10^{-3} D$. LEFT: Spin \uparrow . RIGHT: Spin \downarrow .

The first process consists in attaching the Majorana mode to both Quantum Dots symmetrically. For this, we scale up the coupling parameter $t_1 = t_2$ from 0 (Decoupled) to 0.02 (Completely coupled). The other parameters were chosen with an equilibrium between the dot energy and Coulomb repulsion ($\epsilon_{1,2} = -\frac{U_{1,2}}{2}$) and without inter-dot coupling $t_{dots} = 0$. These circumstances guarantee that the system preserves Particle Hole Symmetry (PHS). Thus the Density of States (DOS) of particles and holes remains equal at all instances ($\rho(-\omega) = \rho(\omega)$).

In the case where the majorana is detached from the DQD ($t_1 = t_2 = 0$), the system favors the appearance of a three-peak at low energies as it is shown in Figure 7.9 . The central peak is produced only by the Kondo effect and the two other satellite peaks are the result of a strong correlation between both dots caused by the indirect exchange of quantum states through the

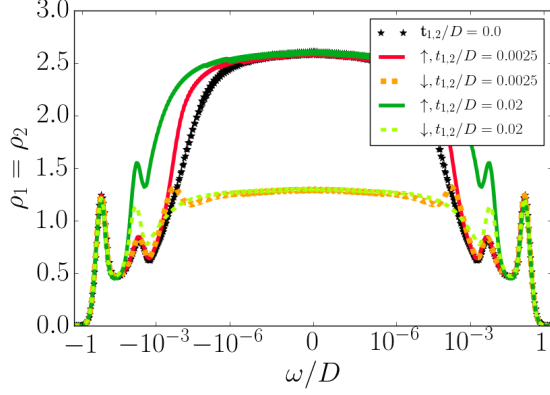


Figure 7.9: Density of states at each QD of the horizontal dashed cuts in Figure 7.8. The energy is in logarithmic scale. For $t_1 = t_2 > 0$ spin- \uparrow and spin- \downarrow DOS split near the order of $|\omega| \sim t_1, 2$. At the Fermi energy ($\omega = 0$) $\rho_\uparrow = 2\rho_\downarrow$ due to the presence of the MZM in both QDs.

Lead Appendix B.

Once the MZM the spin- \uparrow and spin- \downarrow DOS split at low energies due to the new spin- \downarrow transport channel through the Majorana mode. The spin- \downarrow DOS at the Fermi energy ($\omega = 0$) decays to the half of the spin- \uparrow DOS $\rho_\downarrow = \frac{\rho_\uparrow}{2}$. By symmetry in the dot parameters this event occurs equally for both QDs. We adopt this fact as a Majorana signature. Hence we obtain that the MZM leaks inside both quantum dots.

There is also an additional effect caused by the indirect exchange between the QDs through the Majorana mode . The consequences of this effect depend on the energy range of the majorana couplings $t_1 = t_2$. :

1. If $t_1 = t_2 \ll \Gamma$ two more satellites are formed at very low energies ($\sim t_1$) in the spin- \downarrow DOS (See Figure 7.8 Spin-down $\omega \sim 10^{-3}D$). (See Figure 7.8 Spin \uparrow , $\omega \sim 10^{-3}D$).
2. If $t_1 = t_2 \sim \Gamma$, the MZM contributes to the the growth of the spin-up satellites in the DOS. This effect produces the splitting between the spin-up and spin-down DOS. (See Figure 7.8 Spin- \downarrow , $\omega \sim 10^{-2}D$).

7.0.3 e) Transferring the MZM through gate voltage shifting ε_2 .

Parameters:

$$\Gamma \sim 2.83 * 10^{-2}D, t_{dots} = 0, U_{1,2} = -2\varepsilon_1 = 0.5, t_1 = t_2 = 0.0025$$

$$\varepsilon_2 \in [-0.25, -0.05]$$

This process starts with the DQD coupled symmetrically to the Majorana mode, just as in section 7.0.2. The idea of this process is to break PHS by increasing the energy of the second QD ϵ_2 . This procedure should induce the Majorana to tunnel only into the first dot.

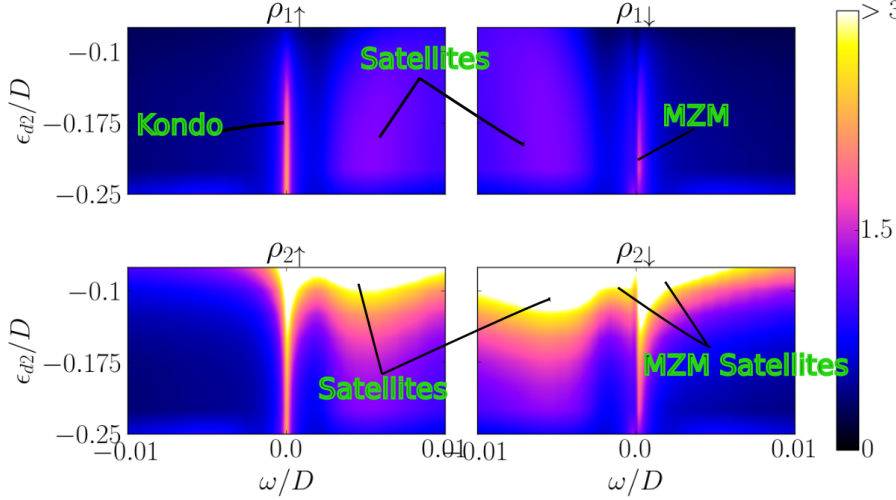


Figure 7.10: Evolution of the DOS of both QDs through the ϵ_2 tuning. UP: QD1. DOWN: QD2. LEFT: Spin \uparrow . RIGHT: Spin \downarrow .

In Figure 7.10 we observe that both, the Kondo and the MZM peaks are preserved in the first QD as well as the majorana signature (See Figure 7.11) when ϵ_2 is scaled up to -0.1 . However, PHS breaking will favor the growth of the spin- \uparrow hole ($w > 0$) satellite and the spin- \downarrow particle ($w < 0$) satellite.

In the second QD the DOS increases abruptly for both spins. The majorana signature is rapidly lost. Hence, with this set-up it is actually possible to induce the Majorana to preferably tunnel QD1 in despite of QD2.

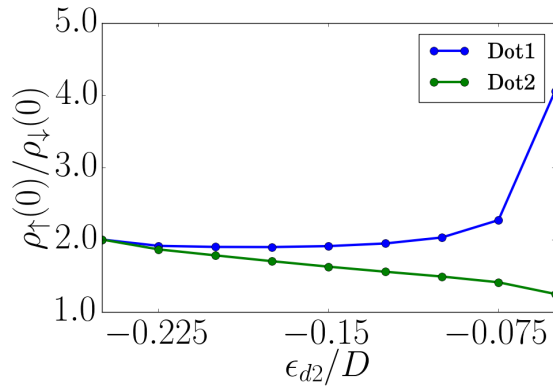


Figure 7.11: As described in section 7.0.2 the relation $\frac{\rho_\uparrow(0)}{\rho_\uparrow(0)} = 2$ constitutes a Majorana Signature . This picture evaluates shows the evolution of the relation $\frac{\rho_\uparrow(0)}{\rho_\uparrow(0)}$ for both QDs. While QD2 losses rapidly the Majorana signature, QD1 maintains it till $\varepsilon_2 \sim -0.1$.

7.1 Particle-Hole symmetric shifting of $\epsilon_2 = \frac{U}{2}$.

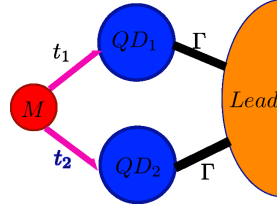


Figure 7.12: $U_1 = -2\epsilon_{d1} = 0.5$, $\Gamma_1 = \Gamma_2$, $t_1 = t_2 = 0.02$. Variable $\epsilon_{d2} = \frac{U_2}{2}$

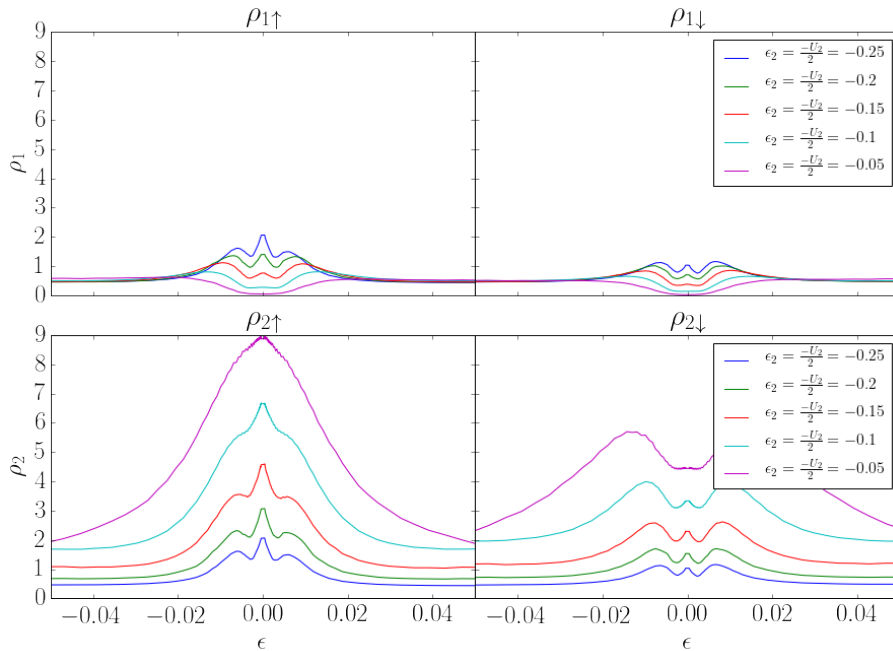


Figure 7.13: Evolution of the QDs' DOS for the model in Figure 7.12

We start again with the symmetric model with both QDs coupled to the Majorana mode, but this time the evolution is performed over $\epsilon_2 = \frac{U}{2}$, such that the model is always Particle-Hole symmetric. This situation is very different from the previous model (subsection 7.0.3) since the decaying of U_2 equalizes the effect of increasing the dot energy. In Figure 7.13 we observe that the DOS of QD2 increases while the QD1's DOS decreases, just as it happened in subsection 7.0.3. However, the Majorana signature remains at 2 for both dots, meaning that the Majorana is not preferably induced to tunnel to any QD despite the loss of symmetry in the dot energy.

7.2 Shifting t_2

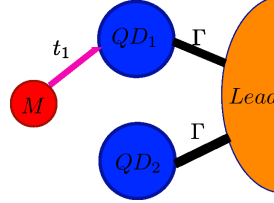


Figure 7.14: $U_1 = U_2 = -2\epsilon_{d1} = -2\epsilon_{d2} = 0.5$, $\Gamma_1 = \Gamma_2$, $t_1 = 0.02$. Variable t_2

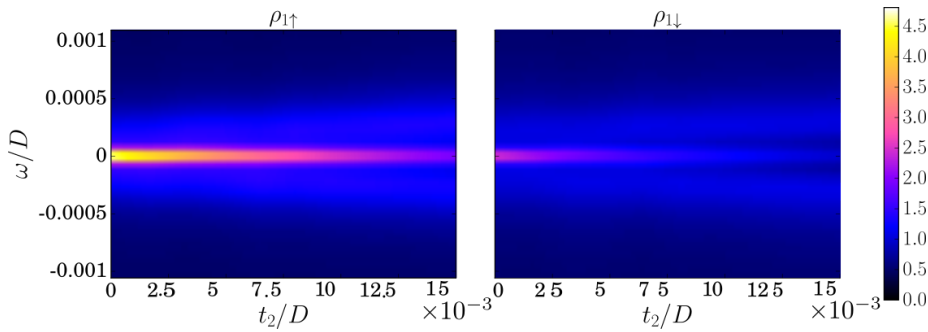


Figure 7.15: Evolution of the DOS in the first QD

In Figure 7.15 and Figure 7.15 we observe the evolution of DOS in the case where the second dot is smoothly connected to the Majorana, which is already attached to the first dot. The hopping parameter t_2 scales up to $0.015D$ where the model reaches the symmetry $t_2 = t_1$. The figures show that increasing t_2 leads to a drop in the DOS of QD1 while the DOS in QD2 is increased. In addition, the single peak in the first dot transforms into a three-peak due to the Majorana interference with the second dot. In ?? we also observe that the ratio between the zero up-down DOS $(\rho_{\uparrow}(0)/\rho_{\downarrow}(0))$ smoothly scales up to 2 in QD2. At $t_2 = 0.02$, when the system is completely symmetric, the Majorana signature appears in both quantum dots. Note that the relation $\frac{\rho_{\uparrow}(0)}{\rho_{\downarrow}(0)}$ is already close to 2 at $t_2 = 0$. This implies that the second dot "feels" the Majorana even when it is not directly connected to the Majorana mode.

Bibliography

- [1] A. Yu Kitaev. Unpaired Majorana fermions in quantum wires. *Phys.-Usp.*, 44(10S):131, 2001. ISSN 1063-7869. doi: 10.1070/1063-7869/44/10S/S29. URL <http://stacks.iop.org/1063-7869/44/i=10S/a=S29>. 1, 3
- [2] Jason Alicea. Majorana fermions in a tunable semiconductor device. *Phys. Rev. B*, 81(12):125318, March 2010. doi: 10.1103/PhysRevB.81.125318. URL <https://link.aps.org/doi/10.1103/PhysRevB.81.125318>. 1
- [3] Jason Alicea. New directions in the pursuit of Majorana fermions in solid state systems. *Rep. Prog. Phys.*, 75(7):076501, 2012. ISSN 0034-4885. doi: 10.1088/0034-4885/75/7/076501. URL <http://stacks.iop.org/0034-4885/75/i=7/a=076501>. 1, 3, 6.1.1, 6.4
- [4] Dong E. Liu and Harold U. Baranger. Detecting a majorana-fermion zero mode using a quantum dot. 84(20). ISSN 1098-0121, 1550-235X. doi: 10.1103/PhysRevB.84.201308. URL <http://arxiv.org/abs/1107.4338>. 1, 3, 6.3
- [5] Minchul Lee, Jong Soo Lim, and Rosa Lopez. Kondo effect in a quantum dot side-coupled to a topological superconductor. 87(24):241402. doi: 10.1103/PhysRevB.87.241402. URL <https://link.aps.org/doi/10.1103/PhysRevB.87.241402>. 1
- [6] E. Vernek, P. H. Penteado, A. C. Seridonio, and J. C. Egues. Subtle leakage of a majorana mode into a quantum dot. 89(16):165314. doi: 10.1103/PhysRevB.89.165314. URL <https://link.aps.org/doi/10.1103/PhysRevB.89.165314>. 1, 3, 6.3, 6.3
- [7] M. T. Deng, S. Vaitiekėnas, E. B. Hansen, J. Danon, M. Leijnse, K. Flensberg, J. Nygård, P. Krogstrup, and C. M. Marcus. Majorana bound state in a coupled quantum-dot hybrid-nanowire system. 354(6319):1557–1562. ISSN 0036-8075, 1095-9203. doi: 10.1126/science.aaf3961. URL <http://science.sciencemag.org/content/354/6319/1557>. 1
- [8] David A. Ruiz-Tijerina, E. Vernek, Luis G. G. V. Dias da Silva, and J. C. Egues. Interaction effects on a majorana zero mode leaking into a quantum dot. 91(11):115435. doi: 10.1103/PhysRevB.91.115435. URL <https://link.aps.org/doi/10.1103/PhysRevB.91.115435>. 1, 3, 3.1, 1, 6.3, 6.3.2

Bibliography

- [9] A. Yu Kitaev. Fault-tolerant quantum computation by anyons. *Annals of Physics*, 303(1):2–30, January 2003. ISSN 00034916. doi: 10.1016/S0003-4916(02)00018-0. URL <http://arxiv.org/abs/quant-ph/9707021>. arXiv: quant-ph/9707021. 3
- [10] Frank Wilczek. Majorana returns, September 2009. URL <https://www.nature.com/articles/nphys1380>. 3
- [11] Liang Fu and C. L. Kane. Superconducting Proximity Effect and Majorana Fermions at the Surface of a Topological Insulator. *Phys. Rev. Lett.*, 100(9):096407, March 2008. doi: 10.1103/PhysRevLett.100.096407. URL <https://link.aps.org/doi/10.1103/PhysRevLett.100.096407>. 3
- [12] Masatoshi Sato, Yoshiro Takahashi, and Satoshi Fujimoto. Non-Abelian Topological Order in \$s\$-\$s\$-Wave Superfluids of Ultracold Fermionic Atoms. *Phys. Rev. Lett.*, 103(2):020401, July 2009. doi: 10.1103/PhysRevLett.103.020401. URL <https://link.aps.org/doi/10.1103/PhysRevLett.103.020401>. 3
- [13] V. Mourik, K. Zuo, S. M. Frolov, S. R. Plissard, E. P. a. M. Bakkers, and L. P. Kouwenhoven. Signatures of Majorana Fermions in Hybrid Superconductor-Semiconductor Nanowire Devices. *Science*, 336(6084):1003–1007, May 2012. ISSN 0036-8075, 1095-9203. doi: 10.1126/science.1222360. URL <http://science-scienmag-org.ez67.periodicos.capes.gov.br/content/336/6084/1003>. 3
- [14] Anindya Das, Yuval Ronen, Yonatan Most, Yuval Oreg, Moty Heiblum, and Hadas Shtrikman. Zero-bias peaks and splitting in an Al-InAs nanowire topological superconductor as a signature of Majorana fermions. *Nature Physics*, 8(12):887, December 2012. ISSN 1745-2481. doi: 10.1038/nphys2479. URL <https://www.nature.com/articles/nphys2479>. 3
- [15] M. T. Deng, C. L. Yu, G. Y. Huang, M. Larsson, P. Caroff, and H. Q. Xu. Anomalous Zero-Bias Conductance Peak in a Nb-InSb Nanowire-Nb Hybrid Device. *Nano Lett.*, 12(12):6414–6419, December 2012. ISSN 1530-6984. doi: 10.1021/nl303758w. URL <http://dx.doi.org/10.1021/nl303758w>. 3
- [16] Yuval Oreg, Gil Refael, and Felix von Oppen. Helical Liquids and Majorana Bound States in Quantum Wires. *Phys. Rev. Lett.*, 105(17):177002, October 2010. doi: 10.1103/PhysRevLett.105.177002. URL <https://link.aps.org/doi/10.1103/PhysRevLett.105.177002>. 3
- [17] Roman M. Lutchyn, Jay D. Sau, and S. Das Sarma. Majorana Fermions and a Topological Phase Transition in Semiconductor-Superconductor Heterostructures. *Phys. Rev. Lett.*, 105(7):077001, August 2010. doi: 10.1103/PhysRevLett.105.077001. URL <https://link.aps.org/doi/10.1103/PhysRevLett.105.077001>. 3

Bibliography

- [18] Alexander Cyril Hewson. *The Kondo Problem to Heavy Fermions*. Cambridge University Press, April 1997. ISBN 978-0-521-59947-4. Google-Books-ID: fPzgHneNFDAC. 3, 4.3
- [19] M. A. Ruderman and C. Kittel. Indirect Exchange Coupling of Nuclear Magnetic Moments by Conduction Electrons. *Physical Review*, 96(1):99–102, October 1954. doi: 10.1103/PhysRev.96.99. URL <https://link.aps.org/doi/10.1103/PhysRev.96.99>. 3, B
- [20] Tadao Kasuya. A Theory of Metallic Ferro- and Antiferromagnetism on Zener’s Model. *Progress of Theoretical Physics*, 16(1):45–57, July 1956. ISSN 0033-068X. doi: 10.1143/PTP.16.45. URL <https://academic.oup.com/ptp/article/16/1/45/1861363>. 3
- [21] Kei Yosida. Magnetic Properties of Cu-Mn Alloys. *Physical Review*, 106(5):893–898, June 1957. doi: 10.1103/PhysRev.106.893. URL <https://link.aps.org/doi/10.1103/PhysRev.106.893>. 3, B
- [22] Luis G. G. V. Dias da Silva, Nancy Sandler, Kevin Ingersent, and Sergio E. Ulloa. Transmission in double quantum dots in the Kondo regime: Quantum-critical transitions and interference effects. *Physica E: Low-dimensional Systems and Nanostructures*, 40(5):1002–1005, March 2008. ISSN 1386-9477. doi: 10.1016/j.physe.2007.08.098. URL <http://www.sciencedirect.com/science/article/pii/S1386947707003074>. 3
- [23] D. N. Zubarev. DOUBLE-TIME GREEN FUNCTIONS IN STATISTICAL PHYSICS. *Soviet Physics Uspekhi*, 3(3):320, 1960. ISSN 0038-5670. doi: 10.1070/PU1960v003n03ABEH003275. URL <http://iopscience.iop.org/article/10.1070/PU1960v003n03ABEH003275/meta>. 3.1
- [24] Kenneth G. Wilson. The renormalization group: Critical phenomena and the Kondo problem. *Reviews of Modern Physics*, 47(4):773–840, October 1975. doi: 10.1103/RevModPhys.47.773. URL <https://link.aps.org/doi/10.1103/RevModPhys.47.773>. 3.1, 5.2
- [25] Alexander W. Holleitner, Robert H. Blick, Andreas K. Härtel, Karl Eberl, and Jürg P. Kotthaus. Probing and Controlling the Bonds of an Artificial Molecule. *Science*, 297(5578):70–72, July 2002. ISSN 0036-8075, 1095-9203. doi: 10.1126/science.1071215. URL <http://science.scienmag.org/content/297/5578/70>. 4.1
- [26] Dieter Bimberg, Marius Grundmann, and Nikolai N. Ledentsov. *Quantum Dot Heterostructures*. Wiley, Chichester, Eng.; New York, 1 edition, March 1999. ISBN 978-0-471-97388-1. 4.1, 4.1
- [27] Michael Sindel. *Numerical Renormalization Group studies of Quantum Impurity Models in the Strong Coupling Limit*. Text.PhDThesis, Ludwig-Maximilians-Universität München, January 2005. URL <https://edoc.ub.uni-muenchen.de/3115/>. 4.1, 4.3, 4.2, 4.3, 5.2

- [28] P. W. Anderson. Localized Magnetic States in Metals. *Physical Review*, 124(1):41–53, October 1961. doi: 10.1103/PhysRev.124.41. URL <https://link.aps.org/doi/10.1103/PhysRev.124.41>. 4.2
- [29] Daniel A Spielman. Algorithms, graph theory, and linear equations in laplacian matrices. In *Proceedings of the International Congress of Mathematicians*, volume 4, pages 2698–2722, 2010. URL <http://www.mathunion.org/ICM/ICM2010.4/Main/icm2010.4.2698.2722.pdf>. 5.1.1, 5.1.1
- [30] H. R. Krishna-murthy, J. W. Wilkins, and K. G. Wilson. Renormalization-group approach to the Anderson model of dilute magnetic alloys. 1. Static properties for the symmetric case. *Phys.Rev.*, B21:1003–1043, 1980. doi: 10.1103/PhysRevB.21.1003. 5.2, 5.2, 5.2, 5.3
- [31] T. A. Costi, A. C. Hewson, and V. Zlatic. Transport coefficients of the Anderson model via the numerical renormalization group. *Journal of Physics: Condensed Matter*, 6(13):2519, 1994. ISSN 0953-8984. doi: 10.1088/0953-8984/6/13/013. URL <http://stacks.iop.org/0953-8984/6/i=13/a=013>. 5.2.1
- [32] Walter Hofstetter. Generalized Numerical Renormalization Group for Dynamical Quantities. *Physical Review Letters*, 85(7):1508–1511, August 2000. doi: 10.1103/PhysRevLett.85.1508. URL <https://link.aps.org/doi/10.1103/PhysRevLett.85.1508>. 5.2.1
- [33] Hao Zhang, Chun-Xiao Liu, Sasa Gazibegovic, Di Xu, John A. Logan, Guanzhong Wang, Nick van Loo, Jouri D. S. Bommer, Michiel W. A. de Moor, Diana Car, Roy L. M. Op het Veld, Petrus J. van Veldhoven, Sebastian Koelling, Marcel A. Verheijen, Mihir Pendharkar, Daniel J. Pennachio, Borzoyeh Shojaei, Joon Sue Lee, Chris J. Palmström, Erik P. A. M. Bakkers, S. Das Sarma, and Leo P. Kouwenhoven. Quantized Majorana conductance. *Nature*, 556:74, March 2018. URL <http://dx.doi.org/10.1038/nature26142>. 6.5

Appendix A

Appendix

A.1 Proof of the Graph Method for Transport Equations.

Appendix B

Three peak appearance in the Double Quantum Dot model.

The DQD model is characterized by the formation of a new state that entangles the two Quantum dots through the leads. This produces an anti-ferromagnetic interaction between the QDs, commonly known as Ruderman-Kittel-Kasuya-Yosida (RKKY) interaction [19, 21]. As consequence, two satellite peaks will emerge in the Density of States.

To explain this phenomenon we will take a symmetric version of Hamiltonian (7.1) with $2e_i = U_i = U$, $t_i = t$ and $t_{dots} = 0$ for $i \in \{1, 2\}$.

$$H = \sum_{i,k,\sigma} \frac{U_i}{2} (d_{i\sigma}^\dagger d_{i\sigma} - 1)^2 + t(d_{+, \downarrow} + d_{+, \uparrow})\gamma_1 + \Gamma_i(d_{i\sigma}^\dagger c_{k\sigma} + c_{k\sigma}^\dagger d_{i\sigma}). \quad (\text{B.1})$$

The symmetry of the previous Hamiltonian is suitable to apply a base change of the form

$$d_{+,\sigma} = \frac{1}{\sqrt{2}}(d_{1\sigma} + d_{2\sigma}), \quad d_{-,\sigma} = \frac{1}{\sqrt{2}}(d_{1\sigma} - d_{2\sigma}).$$

These new operators satisfy the fermionic anti-commutation relations

$$\{d_{\pm,\sigma}, d_{\pm,\sigma}^\dagger\} = 1, \{d_{\pm,\sigma}, d_{\mp,\sigma}^\dagger\} = 0,$$

so that they may be considered as fermion operators. All lineal terms in (B.1) are trivially adapted to the new base. The repulsion potential

$$\sum_i (\sum_\sigma d_{i\sigma}^\dagger d_{i\sigma} - 1)^2 = (\sum_\sigma d_{1\sigma}^\dagger d_{1\sigma} - 1)^2 + (\sum_\sigma d_{2\sigma}^\dagger d_{2\sigma} - 1)^2.$$

gives rise to a non-trivial interaction between the new states. To find this interaction we define the particle number operator

$$\hat{n}_{i,\sigma} := d_{i,\sigma}^\dagger d_{i,\sigma}.$$

So that

$$\hat{n}_{1,\sigma} = \frac{1}{2} (\hat{n}_{+,\sigma} + \hat{n}_{-,\sigma} + d_{+,\sigma}^\dagger d_{-,\sigma} + d_{-,\sigma}^\dagger d_{+,\sigma}) = \frac{1}{2} (\hat{N}_\sigma + \hat{E}_\sigma),$$

with $\hat{N} = \hat{n}_{+,\sigma} + \hat{n}_{-,\sigma}$ and $\hat{E}_\sigma = d_{+,\sigma}^\dagger d_{-,\sigma} + d_{-,\sigma}^\dagger d_{+,\sigma}$. Similarly

$$\hat{n}_{2,\sigma} = \frac{1}{2} (\hat{N}_\sigma - \hat{E}_\sigma).$$

Hence

$$\sum_i \left(\sum_{\sigma} d_{i\sigma}^{\dagger} d_{i\sigma} - 1 \right)^2 = \left(\frac{\hat{N} + \hat{E}}{2} - 1 \right)^2 + \left(\frac{\hat{N} - \hat{E}}{2} - 1 \right)^2 = \frac{(\hat{N} - 2)^2 - \hat{E}^2}{2},$$

with $\hat{N} = \sum_{\sigma} \hat{N}_{\sigma}$, $\hat{E} = \sum_{\sigma} \hat{E}_{\sigma}$. Note that opeator \hat{N} represents the total occupation number inside both dots. If this occupation is different than 2 there is an imbalance between particles and dots that is punished by this term. The term E^2 is much more interesting since this one is the responsible for the emergence of satellite peaks in the DOS. To understand what it makes it is simple to observe its results when applied to a based ordered by $|+, -\rangle$.

$$\begin{aligned} \hat{E}^2 |\uparrow, 0\rangle &= \hat{E} |0, \uparrow\rangle = |\uparrow, 0\rangle \\ \hat{E}^2 |\uparrow, \downarrow\rangle &= \hat{E} (|0, \uparrow\downarrow\rangle + |\uparrow\downarrow, 0\rangle) = 2|\uparrow, \downarrow\rangle - 2|\downarrow, \uparrow\rangle \end{aligned}$$

The new Hamiltonian

$$H = \sum_{\sigma} \frac{U}{4} \left((\hat{N} - 2)^2 - \hat{E}^2 \right) + \frac{t}{\sqrt{2}} (d_{+, \downarrow} + d_{+, \downarrow}^{\dagger}) \gamma_1 + \frac{\Gamma}{\sqrt{2}} \sum_k (d_{+, \sigma}^{\dagger} c_{k\sigma} + c_{k\sigma}^{\dagger} d_{+, \sigma}) \quad (\text{B.2})$$

is represented in ??

We can explain this three-peak as the result of a new strong coupling interaction characterized by the spin exchange between both dots.

In addition, the spin-up DOS at the Fermi energy grows faster than the spin-down DOS, breaking the initial spin-symmetry when $t_1 = t_2 = 0$. At $t_1 = t_2 = 0.02D$ the spin-up DOS at the fermi energy doubles the spin-down DOS which implies that the Majorana signature is present in both dots. Indeed ?? shows that the relation $\frac{\rho_{\uparrow}(0)}{\rho_{\uparrow}(0)}$ increases continuously from 1 to 2. Note that the Majorana is completely attached when the coupling t_1 reaches the order of $0.01D$.

B.1 Initial DQD-Majorana Hamiltonian.

$H_{N_{\uparrow}=0, P_{\downarrow}=-1}$:

$$\begin{aligned} |\downarrow, \downarrow, \downarrow\rangle &\rightarrow \left[\begin{array}{cccc} \varepsilon_d^+ + \frac{U^+}{2} - 2h + \varepsilon_m & 0 & -\tilde{t}_{+1} & \tilde{t}_{+2} \\ 0 & \frac{U^+}{2} + \varepsilon_m & \tilde{t}_{-2}^* & \tilde{t}_{-1}^* \\ 0, \downarrow, 0\rangle & \rightarrow \left[\begin{array}{cccc} -\tilde{t}_{+1}^* & \tilde{t}_{-2} & \varepsilon_{d_2} + \frac{U^+}{2} - h - \varepsilon_m & t \\ \tilde{t}_{+2}^* & \tilde{t}_{-1} & t^* & \varepsilon_{d_1} + \frac{U^+}{2} - h - \varepsilon_m \end{array} \right] \\ |\downarrow, 0, 0\rangle &\rightarrow \left[\begin{array}{cccc} \varepsilon_d^+ + \frac{U^+}{2} - 2h - \varepsilon_m & 0 & \tilde{t}_{+1} & \tilde{t}_{+2} \\ 0 & \varepsilon_d^+ + \frac{U^+}{2} - 2h - \varepsilon_m & \tilde{t}_{-2}^* & -\tilde{t}_{-1}^* \\ \tilde{t}_{+1}^* & \tilde{t}_{-2} & \varepsilon_{d_1} + \frac{U^+}{2} - h + \varepsilon_m & t \\ \tilde{t}_{+2}^* & -\tilde{t}_{-1} & t^* & \varepsilon_{d_2} + \frac{U^+}{2} - h + \varepsilon_m \end{array} \right] \end{aligned}$$

$H_{N_{\uparrow}=0, P_{\downarrow}=1}$:

$$\begin{aligned} |0, 0, 0\rangle &\rightarrow \left[\begin{array}{cccc} \frac{U^+}{2} - \varepsilon_m & 0 & \tilde{t}_{+1} & \tilde{t}_{+2} \\ 0 & \varepsilon_d^+ + \frac{U^+}{2} - 2h - \varepsilon_m & \tilde{t}_{-2}^* & -\tilde{t}_{-1}^* \\ |\downarrow, \downarrow, 0\rangle & \rightarrow \left[\begin{array}{cccc} \tilde{t}_{+1}^* & \tilde{t}_{-2} & \varepsilon_{d_1} + \frac{U^+}{2} - h + \varepsilon_m & t \\ \tilde{t}_{+2}^* & -\tilde{t}_{-1} & t^* & \varepsilon_{d_2} + \frac{U^+}{2} - h + \varepsilon_m \end{array} \right] \\ |\downarrow, 0, \downarrow\rangle &\rightarrow \left[\begin{array}{cccc} \varepsilon_d^+ + \frac{U^+}{2} - 2h - \varepsilon_m & 0 & \tilde{t}_{+1} & \tilde{t}_{+2} \\ 0 & \varepsilon_d^+ + \frac{U^+}{2} - 2h - \varepsilon_m & \tilde{t}_{-2}^* & -\tilde{t}_{-1}^* \\ \tilde{t}_{+1}^* & \tilde{t}_{-2} & \varepsilon_{d_1} + \frac{U^+}{2} - h + \varepsilon_m & t \\ \tilde{t}_{+2}^* & -\tilde{t}_{-1} & t^* & \varepsilon_{d_2} + \frac{U^+}{2} - h + \varepsilon_m \end{array} \right] \end{aligned}$$

B.1. Initial DQD-Majorana Hamiltonian.

$H_{N_\uparrow=2, P_\downarrow=-1}$:

$$\begin{aligned} |\uparrow\downarrow, \uparrow\downarrow, \downarrow\rangle &\rightarrow \left[\begin{array}{cccc} 2\epsilon_d^+ + \frac{3U^+}{2} + \epsilon_m & 0 & \tilde{t}_{+1} & \tilde{t}_{+2} \\ 0 & \epsilon_d^+ + \frac{U^+}{2} + 2h + \epsilon_m & \tilde{t}_{-2}^* & -\tilde{t}_{-1}^* \\ \tilde{t}_{+1}^* & \tilde{t}_{-2} & f(d_1, d_2) + h - \epsilon_m & -t \\ \tilde{t}_{+2}^* & -\tilde{t}_{-1} & -t^* & f(d_2, d_1) + h - \epsilon_m \end{array} \right] \\ |\uparrow\uparrow, \downarrow\downarrow\rangle &\rightarrow \\ |\uparrow\uparrow, \downarrow\downarrow, 0\rangle &\rightarrow \\ |\uparrow\downarrow, \uparrow\downarrow, 0\rangle &\rightarrow \end{aligned}$$

with $f(d_i, d_j) = \epsilon_{d_i} + \frac{U_i}{2} + 2\epsilon_{d_j} + \frac{3U_j}{2}$.

$H_{N_\uparrow=2, P_\downarrow=1}$:

$$\begin{aligned} |\uparrow, \uparrow, 0\rangle &\rightarrow \left[\begin{array}{cccc} \epsilon_d^+ + \frac{U^+}{2} + 2h - \epsilon_m & 0 & -\tilde{t}_{+1} & \tilde{t}_{+2} \\ 0 & 2\epsilon_d^+ + \frac{3U^+}{2} - \epsilon_m & \tilde{t}_{-2}^* & \tilde{t}_{-1}^* \\ -\tilde{t}_{+1}^* & \tilde{t}_{-2} & f(d_2, d_1) + h + \epsilon_m & -t \\ \tilde{t}_{+2}^* & \tilde{t}_{-1} & -t^* & f(d_1, d_2) + h + \epsilon_m \end{array} \right] \\ |\uparrow\downarrow, \uparrow\downarrow, 0\rangle &\rightarrow \\ |\uparrow\downarrow, \uparrow\downarrow, \downarrow\rangle &\rightarrow \\ |\uparrow, \uparrow\downarrow, \downarrow\rangle &\rightarrow \end{aligned}$$